Entanglement of nitrogen-vacancy-center ensembles with initial squeezing

Andri Pradana [1] and Lock Yue Chew [1,2,3,*]

[1] *Division of Physics and Applied Physics, School of Physical and Mathematical Sciences, 21 Nanyang Link, Nanyang Technological University, Singapore 637371*

[2] *Data Science and Artificial Intelligence Research Centre, Block N4 #02a-32, Nanyang Avenue, Nanyang Technological University, Singapore 639798*

[3] *Complexity Institute, 61 Nanyang Drive, Nanyang Technological University, Singapore 637335*

(Received 28 December 2020; revised 9 July 2021; accepted 13 August 2021; published 27 August 2021)

In this paper, we investigate entanglement of an experimental system of two nitrogen-vacancy-center ensembles which are initially squeezed under the one-axis twisting Hamiltonian. We take into account three scenarios in which initial squeezing and entanglement are mediated by phonons or photons: (a) the phonon-squeezed photon-entangled scenario, (b) the phonon-squeezed phonon-entangled scenario, and (c) the photon-squeezed photon-entangled scenario. For our investigation, we employ the Tavis-Cummings model, which includes dissipative decoherence of the collective spin ensemble, and analyze the system both for a relatively small number of spins and in the limit of a large number of spins using the approach of a quantum master equation. Although evidence in the literature on idealized coupled oscillator systems and coupled quantum kicked tops suggests that initial squeezing can enhance entanglement, we find that, in the realistic system studied in this paper, initial squeezing can improve entanglement overall when the field mode interacts in a particular manner with the two spin ensembles. Our analysis using the Holstein-Primakoff transformation and Wigner characteristic function in the rotating frame of reference shows that the entanglement enhancement is a subtle consequence of the way in which the dissipative decoherence rotates the state of the collective spin ensemble such that enhancement depends on the time-evolved rotated states between the presence and absence of initial squeezing.

DOI: 10.1103/PhysRevA.104.022435

I. INTRODUCTION

Recently, there has been active interest in realizing quantum information processing in quantum networks. A quantum network is formed by quantum nodes and quantum links. Quantum nodes contain quantum processors and quantum memories which are typically made up of matter systems such as trapped ions, single atoms, atomic ensembles, and solid-state systems, while quantum links are mediated through bosonic particles such as photons since their transmission through fiber-optic links is more robust against decoherence. One important quantum information processing task in a quantum network is the generation of quantum entanglement between nodes through the quantum processors or memories interacting via the quantum link. The quantum entanglement generated becomes a resource for quantum protocols relating to quantum communication and computation such as quantum teleportation and constitutes a storage of nonclassical states useful for other quantum computing tasks involving quantum repeaters and quantum metrology.

A basic unit of a quantum network is two quantum nodes connected by a quantum link. An amalgamation of this basic unit forms a complex network of diverse network topology according to the manner in which the units are connected with each other. In this paper, we are concerned with the study of such a basic unit with the specific condition that the two quantum nodes are of the same type and mediated by bosonic mode fields. In particular, we consider the use of a spin ensemble as the key component in the quantum node, with the basis of the ensemble being the spin state that arises from the nitrogen-vacancy (NV) center. The NV center [1] is a type of defect in diamond, with a carbon atom replaced by a nitrogen atom, next to a vacancy. It has a long coherence time [2–4] and excellent optical properties [5–7], which make the NV center attractive for implementation of quantum information applications, one of which is generating entanglement. Quantum entanglement of the NV center with photons [8], between single spins [9,10] and between ensembles [11], has already been demonstrated in the literature.

A useful operation on the NV-center ensembles is spin squeezing [12]. Spin squeezing, first introduced by Kitagawa and Ueda [13], is quantum redistribution of the uncertainties of two orthogonal spin directions. Spin squeezing is an important tool in quantum sensing and metrology; it allows for improvement in measurement precision in experiments beyond the standard quantum limit [14–18]. Thus, spin squeezing is a resource in quantum technology applications. It is commonly applied particularly for sensing and in enhancing the precision of measurement.

Spin squeezing and entanglement are intrinsically related. It is known that in ensemble of spins, a squeezed state occurs when there is many-body entanglement between the constituent spins [19,20]. Spin squeezing that

*lockyue@ntu.edu.sg

occurs within this ensemble or single collective state is also known as single-mode spin squeezing. Two-mode spin squeezing is the entanglement between two separate ensembles of spins [21–23]. This concept has been explored and implemented, for example, in characterizing multibody entanglement by spin squeezing [20,24–26], in spin squeezing of atomic ensembles via nuclear-electronic spin entanglement [27], and in spin squeezing of atoms via entanglement of light with atoms [28–31]. However, work on the application of prior single-mode spin squeezing to enhance dynamically generated entanglement of two separate NV-center spin ensembles is lacking.

In this paper, we consider an application of prior single-mode spin squeezing of two separate NV-center ensembles to enhance the subsequent entanglement generated between the two ensembles. This is motivated by theoretical studies on idealized coupled oscillator systems [32–35] and coupled quantum kicked tops [36] that give credence to the idea that implementing prior squeezing could enhance entanglement in practical systems. However, as we will see, this is not always true in our case. For this purpose, we consider an experimentally realizable entanglement of NV-center ensembles via a cavity bus or transmission line resonator as in Ref. [11]. Thus, the systems studied here are realistic and relevant for experiments.

In essence, the negatively charged NV center that we consider has a ground state of a spin triplet $|m_s = 0, \pm 1\rangle$ [37], with a zero-field splitting of $D_0 \approx 2.88$ GHz between $|m_s = 0\rangle$ and $|m_s = \pm 1\rangle$ states. With the external magnetic field aligned along the NV axis B_z, the Zeeman splitting of the $|m_s = \pm 1\rangle$ states is $\Delta_B = g_e \mu_B B_z/\hbar$, where $g_e \approx 2$ is the electron's g factor and μ_B is the Bohr magneton. With preparation of the NV-center ensemble in the $|m_s = \pm 1\rangle$ subspace and under the condition of nearly resonant coupling, in which detuning $\Delta = \Delta_B - \omega \ll D_0$, the state $|m_s = 0\rangle$ remains unpopulated. Therefore, the system can generally be treated as a two-level spin-ensemble system. Our purpose would be to first spin squeeze two such NV-center ensembles separately, before entangling them through their interaction with a channel of bosonic particles. We aim to investigate the effect of the initial spin squeeze on the subsequent entanglement between the spin ensembles.

Theoretically, we could spin squeeze the two NV-center ensembles with phonons or photons and then entangle them via phonons or photons, giving rise to four possible configurations. Combining the idea of the spin squeezing of the NV-center ensemble by phonons from the nanomechanical resonator system in Ref. [12] and the entanglement between ensembles via coupling with photons in the cavity quantum electrodynamics system in Ref. [11], we create the scenario where two separate NV-center ensembles are individually squeezed first by phonons before the two ensembles are entangled by photons. We call this scenario the phonon-photon scenario.

However, the coupling strength of a single NV center in the nanomechanical resonator system is on the order of $g_m/2\pi \sim 1$ kHz [12], while the coupling strength in the cavity resonator system is much smaller, about $g_c/2\pi \sim 10$ Hz. This small coupling strength may pose as a limitation, especially for the relatively small number of spins ($N \sim 50$–100) considered in Ref. [12]. This can be alleviated if we theoretically consider that entanglement is mediated by phonons, with the higher associated coupling strength. This will be referred to as the phonon-phonon scenario, in which initial squeezing and then entanglement are both mediated by phonons in a mechanical resonator system.

Another possibility is to increase the number of spins to increase the collective coupling strength, as the collective coupling strength scales with $\sqrt{N}$ [38]. A strong coupling of approximately 10 MHz has been reported for an ensemble of $N \sim 10^{12}$ NV centers in a cavity resonator system [39,40]. However, increasing the number of NV centers has an adverse effect on the coupling strength g_m, since it was shown in Ref. [12] that increasing the size of the resonator beam (to have more NV centers) will reduce the individual coupling strength. Hence, it does not make physical sense to implement the photon-phonon scenario, i.e., squeezing first by photons before entanglement by phonons. On the other hand, this restriction can be eliminated if we consider that initial squeezing and entanglement are both achieved with the cavity resonator. This scenario will be referred to as the photon-photon scenario. This is perhaps the most realistic and practical scenario since the cavity resonator system has been widely studied and implemented and there is little to no change in the setup between the initial individual squeezing and entanglement.

Our paper is organized as follows. In Sec. II we present the models and frameworks of the Hamiltonians and decoherence. We find that both the squeezing and entanglement Hamiltonians generally follow the Tavis-Cummings model [41]. On the other hand, the form of the dissipative decoherence depends on whether it is phonons or photons that mediate the interaction. Section III gives the methodology we employ to analyze the system with the goal of obtaining the time evolution under the corresponding Hamiltonians and decoherence. As mentioned previously, in the phonon-photon and phonon-phonon scenarios, the number of spins involved is relatively small, $N \sim 50$–100 in each ensemble. However, in the photon-photon scenario, the number of spins is much larger, $N \sim 10^{12}$ in each ensemble. Naturally, different approaches are required to simulate the system based on the number of spins involved. As a result, we examine separately the approach for small N for the phonon-photon and phonon-phonon scenarios and the limit of large N for the photon-photon scenario. After a detailed analysis of each of the three scenarios, we present and discuss the results obtained in Sec. IV. We summarize and give our conclusions in Sec. V.

II. MODELS

A. Hamiltonians and the dispersive regime

Both the nanomechanical resonator system [12] and cavity resonator system [11] follow the Tavis-Cummings model, which describes interactions between the spins and a resonator field mode. This makes it possible to have a generalized description for the squeezing and entanglement Hamiltonians for the different scenarios. Furthermore, we consider the dispersive regime which results in effective spin-spin interaction. This will be explained later.

1. Squeezing Hamiltonian

Following the Tavis-Cummings model, the Hamiltonian for a single ensemble is given by ($\hbar = 1$)

$$H = \omega a^\dagger a + \Delta_B J_z + g(aJ_+ + a^\dagger J_-), \tag{1}$$

where $a^\dagger$ and a are the creation and annihilation operators for the resonator mode corresponding to frequency ω, g is the coupling constant of the interaction term, $J_z = 1/2\sum_{i=1}^{N}\sigma_i^z$ and $J_\pm = \sum_{i=1}^{N}\sigma_i^\pm$ are the collective spin operators, and N is the total number of spins. Note that the coupling for each of the spins within each ensemble may be nonuniform. In this case, the effective coupling constant is $g_{\text{eff}} = \sqrt{\sum_{i=1}^{N} g_i^2/N}$, with collective spin operators $J_{\text{col}}^\pm = \sum_{i=1}^{N}(g_i/g_{\text{eff}})\sigma_i^\pm$ [11]. With the distribution of g_i, it was noted in Ref. [12] that the effective length of the collective spin involved in the dynamics becomes $(\sum_i g_i)^2/2\sum_i g_i^2$, which is $\frac{N}{2}$ for uniform coupling. This in turn means that the effective number of spins is reduced, that is, $N_{\text{eff}} < N$. Therefore, we approximate the effective collective spin operators to $J_{\text{eff}}^\pm = \sum_{i=1}^{N_{\text{eff}}}\sigma_i^\pm$. For compactness of notation, we drop the subscript eff, but in essence we are considering the effective quantities and operators. Hence, in the preceding and following discussions, the number of spins N in an ensemble refers to the effective number of spins.

In the dispersive regime, the detuning is large, $\Delta = \Delta_B - \omega \gg \sqrt{N}g$, and the interaction term in the Hamiltonian can be considered as a small perturbation. Let V denote the small perturbation, so $V = g(aJ_+ + a^\dagger J_-)$, and let H_0 be the resonator and ensemble energy terms, so $H_0 = \omega a^\dagger a + \Delta_B J_z$. Under this condition, the Schrieffer-Wolff transformation [42,43] can be applied, which is a unitary transformation $e^S H e^{-S}$. With the generator S chosen such that $[H_0, S] = V$, the unitary transformation can be approximated by $H' = e^S H e^{-S} \approx H_0 + \frac{1}{2}[S, V]$. Therefore, with the appropriate choice of generator

$$S = \frac{g}{\Delta}(aJ_+ - a^\dagger J_-), \tag{2}$$

applying the transformation up to order $(g/\Delta)^2$ yields

$$H' = \omega a^\dagger a + \Delta_B J_z + \frac{g^2}{\Delta}(J_+J_- + 2a^\dagger a J_z). \tag{3}$$

The transformation represents a change of frame. Since the resonator mode is far detuned from the transition energy of the ensemble, $\langle a^\dagger a\rangle \sim 0$ in this frame [44]. Thus, it effectively eliminates the direct resonator field-spin coupling and the Hamiltonian can then be projected on the spin-ensemble subspace [45], resulting in the effective projected Hamiltonian

$$H_{\text{sq}} = \Delta_B J_z + \frac{g^2}{\Delta}J_+J_- = \Delta_B J_z + \frac{g^2}{\Delta}\left(\mathbf{J}^2 + J_z - J_z^2\right), \tag{4}$$

where $\mathbf{J}$ is the total collective spin vector operator. The term proportional to J_z^2 corresponds to the one-axis twisting Hamiltonian, originally introduced by Kitagawa and Ueda [13], that provides the underlying mechanism for spin squeezing. Projection of the Hamiltonian on the spin subspace is computationally advantageous since the infinite-dimensional Hilbert space of the mechanical mode is projected out, leaving only the finite-dimensional spin subspace, which can be more easily simulated, especially for relatively small N. If spin squeezing is mediated by phonons (photons), the corresponding coupling constant is g_m (g_c).

2. Entanglement Hamiltonians

The Hamiltonian following the Tavis-Cummings model with two spin ensembles, according to Ref. [11], is given by

$$\begin{aligned} H = {} & \omega a^\dagger a + \Delta_{B1}J_1^z + \Delta_{B2}J_2^z \\ & + g_1(aJ_1^+ + a^\dagger J_1^-) - g_2(aJ_2^+ + a^\dagger J_2^-), \end{aligned} \tag{5}$$

where subscripts 1 and 2 denote the two ensembles. The opposite signs of the coupling terms is due to the fact that the field of the resonator mode interacting with one ensemble has the opposite sign or direction from the other ensemble in the setup [11]. For simplicity, we consider two approximately identical NV-center ensembles with Zeeman splitting $\Delta_{B1} \approx \Delta_{B2} \approx \Delta_B$, coupling constant $g_1 \approx g_2 \approx g$, and total number of spins $N_1 \approx N_2 \approx N$. So the Hamiltonian can be simplified to

$$H = \omega a^\dagger a + \Delta_B\left(J_1^z + J_2^z\right) + g[a(J_1^+ - J_2^+) + a^\dagger(J_1^- - J_2^-)]. \tag{6}$$

Here the detuning is $\Delta = \Delta_B - \omega$.

In the dispersive regime, the appropriate generator of transformation for this Hamiltonian is given by

$$S = \frac{g}{\Delta}[a(J_1^+ - J_2^+) - a^\dagger(J_1^- - J_2^-)]. \tag{7}$$

Applying the Schrieffer-Wolff transformation yields

$$\begin{aligned} H' = {} & \omega a^\dagger a + \Delta_B\left(J_1^z + J_2^z\right) + \frac{2g^2}{\Delta}a^\dagger a\left(J_1^z + J_2^z\right) \\ & + \frac{g^2}{\Delta}(J_1^+J_1^- + J_2^+J_2^- - J_1^+J_2^- - J_2^+J_1^-). \end{aligned} \tag{8}$$

Similar to before, this Hamiltonian can be projected onto the spin subspace, which gives the effective Hamiltonian

$$H_{\text{ent},-} = \Delta_B\left(J_1^z + J_2^z\right) + \frac{g^2}{\Delta}(J_1^+J_1^- + J_2^+J_2^- - J_1^+J_2^- - J_2^+J_1^-). \tag{9}$$

Thus, the dispersive regime results in direct ensemble-ensemble coupling mediated by virtual photons or phonons.

As mentioned previously, in Eq. (5) the opposite signs of the coupling terms is due to the opposite sign or direction of the field mode interacting with the different ensembles. In addition, it is also conceivable to have a different experimental setup in which the coupling terms have the same sign. Therefore, we also consider this possibility with the Hamiltonian given by

$$\begin{aligned} H = {} & \omega a^\dagger a + \Delta_B\left(J_1^z + J_2^z\right) \\ & + g[a(J_1^+ + J_2^+) + a^\dagger(J_1^- + J_2^-)]. \end{aligned} \tag{10}$$

In the dispersive regime, the appropriate generator of transformation for this Hamiltonian is given by

$$S = \frac{g}{\Delta}[a(J_1^+ + J_2^+) - a^\dagger(J_1^- + J_2^-)]. \tag{11}$$

Applying the Schrieffer-Wolff transformation yields

$$H' = \omega a^\dagger a + \Delta_B\left(J_1^z + J_2^z\right) + \frac{2g^2}{\Delta} a^\dagger a\left(J_1^z + J_2^z\right) + \frac{g^2}{\Delta}(J_1^+ J_1^- + J_2^+ J_2^- + J_1^+ J_2^- + J_2^+ J_1^-). \quad (12)$$

Projecting the Hamiltonian onto the spin subspace gives

$$H_{\mathrm{ent},+} = \Delta_B\left(J_1^z + J_2^z\right) + \frac{g^2}{\Delta}(J_1^+ J_1^- + J_2^+ J_2^- + J_1^+ J_2^- + J_2^+ J_1^-). \quad (13)$$

Therefore, we consider two entanglement schemes in the form of $H_{\mathrm{ent},-}$ and $H_{\mathrm{ent},+}$. If entanglement is mediated by phonons (photons), the corresponding coupling constant is g_m (g_c).

B. Decoherence

Interaction between the resonators and environment induces energy dissipation in the form of heat. This dissipative decoherence is expressed as coupling of the resonator mode with the environment, which is defined by a master equation describing the time evolution of the system density operator $\dot{\rho}$. Depending on whether it is phonons or photons that mediate the spin squeezing and/or entanglement dynamics of the resonator system, the decoherence may take different forms. Moreover, since the dispersive regime is considered, the master equation for the decoherence is also transformed by the generator S used previously to obtain the effective Hamiltonian.

To summarize, there are two master equations for decoherence corresponding to phonons and photons. In addition, since we consider a variation of scenarios in which phonons and photons may mediate both spin squeezing and entanglement, in the dispersive regime each of the master equations has three possible transformations, corresponding to the generators in Eqs. (2), (7), and (11).

To organize and make the notation more compact, let us introduce a generalized form for the generator of transformation

$$S = \frac{g}{\Delta}(aF^\dagger - a^\dagger F). \quad (14)$$

Here F can take different forms depending on each case: $F = J_-$ in Eq. (2), $F = J_1^- - J_2^-$ in Eq. (7), or $F = J_1^- + J_2^-$ in Eq. (11).

We will denote the time evolution due to decoherence by $\dot{\rho}_D$. So, in addition to the dynamics of the Hamiltonian, the full master equation of the system can be written as $\dot{\rho} = -i[H, \rho] + \dot{\rho}_D$.

First, the master equation for dissipation in the optical resonator is given by

$$\dot{\rho}_D = \kappa \mathcal{D}[a]\rho, \quad (15)$$

where $\mathcal{D}[K]\rho = K\rho K^\dagger - \frac{1}{2}(K^\dagger K\rho + \rho K^\dagger K)$, $\kappa = \omega_c/Q$ is the damping rate, ω_c is the resonant frequency of the optical mode, and Q is the quality factor. Applying the unitary transformation $e^S \dot{\rho} e^{-S}$ in the dispersive regime up to order $(g_c/\Delta)^2$ and projecting onto the spin subspace yields

$$\dot{\rho}_{D,c} = \left(\frac{g_c}{\Delta}\right)^2 \kappa \mathcal{D}[F]\rho. \quad (16)$$

Next, mechanical dissipation in mechanical resonator is given by [12]

$$\dot{\rho}_D = \gamma(\bar{n}_{th} + 1)\mathcal{D}[a]\rho + \gamma \bar{n}_{th}\mathcal{D}[a^\dagger]\rho, \quad (17)$$

where $\gamma = \omega_m/Q$ is the damping rate, ω_m is the resonant frequency of the mechanical mode, Q is the quality factor, and $\bar{n}_{th} = [\exp(\hbar\omega_m/k_B T) - 1]^{-1}$ is the average thermal phonon number at temperature T. The dependence on temperature here makes the system more susceptible to decoherence at higher temperatures. Applying the transformation in the dispersive regime up to order $(g_m/\Delta)^2$ and projecting onto the spin subspace yields

$$\dot{\rho}_{D,m} = \left(\frac{g_m}{\Delta}\right)^2 \gamma(\bar{n}_{th} + 1)\mathcal{D}[F]\rho + \left(\frac{g_m}{\Delta}\right)^2 \gamma \bar{n}_{th}\mathcal{D}[F^\dagger]\rho. \quad (18)$$

The resulting master Eqs. (16) and (18) can be regarded as collective spin relaxation. Thus, dissipative decoherence induces collective spin relaxation through interaction with the resonator mode.

Apart from the decoherence discussed above, an individual NV-center spin also experiences intrinsic decoherence due to its interaction with its surroundings. One type of interaction is spin-lattice interaction with the associated relaxation time T_1. However, T_1 can be very long, on the order of hundreds of seconds at low temperature [46]. Therefore, we may ignore this type of decoherence. The other type is magnetic interaction with the surrounding electronic and nuclear spins [47,48], with an associated coherence time T_2^*. This coherence time can be further extended by employing techniques [49–52] that effectively reduce the effects of interaction. In particular, an extended coherence time $T_2 \sim 0.6$ s has been achieved by employing dynamical decoupling using an isotopically pure sample (0.01% ^{13}C) at 77 K [3]. In the following, we also ignore this type of decoherence. We analyze dynamical decoupling for $N = 6$ in Appendix B to show that this is a good approximation, especially for the maximum achievable entanglement, as long as the timescale involved is less than $T_2 \sim 0.6$ s (up to 0.1 s in our case). Obviously, if the entanglement timescale is much longer than the coherence time T_2, then no significant entanglement can be achieved. Therefore, the entanglement timescale needs to be examined in the results, which are given in Sec. IV for each of the scenarios considered.

C. Parameters

Here we give some important parameters required to perform the calculation. For the nanomechanical resonator [12], the average thermal phonon number at temperature T is $\bar{n}_{th} = [\exp(\hbar\omega_m/k_B T) - 1]^{-1}$. Assuming $\omega_m/2\pi \sim 1$ GHz for $\bar{n}_{th} = 1$ gives $T \sim 70$ mK. An operational temperature of tens of millikelvin for an NV-center ensemble in diamond is achievable and was demonstrated, for example, in Refs. [40,53]. Quality factors Q for nanomechanical resonator have been reported for about 10^4 [54,55], 10^5 [56], and 10^6 at millikelvin temperatures [57]. Here we take $Q \sim 10^5$.

For the cavity resonator system, we similarly assume temperature to be in the tens of millikelvin range. The quality factor is assumed to be $Q \sim 10^3$, following Ref. [11].

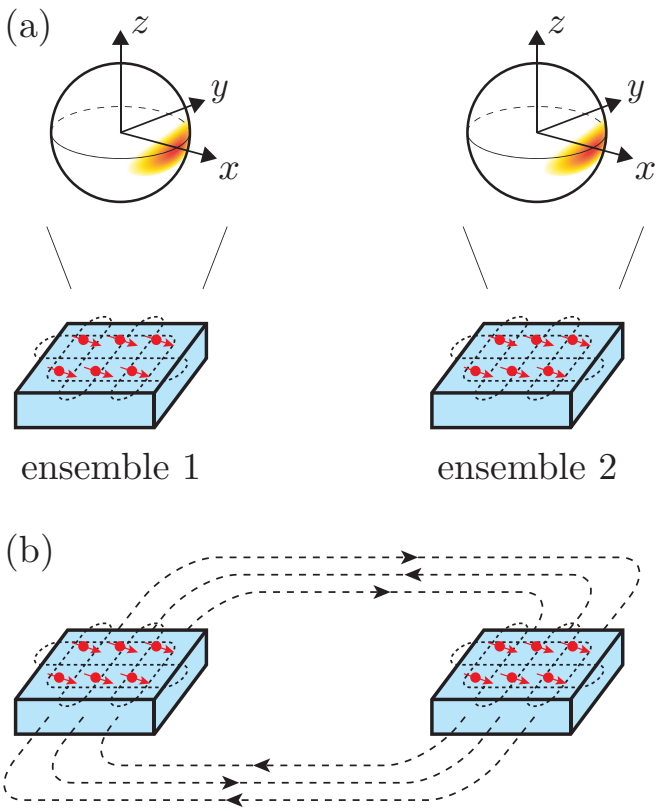

FIG. 1. Conceptual illustration of the process. (a) Two separate spin ensembles are individually squeezed first, as can be seen in the Bloch sphere depiction of the spin uncertainty distribution. Dotted lines indicate interaction in the form of local squeezing. (b) Afterward, the two ensembles are entangled. Dashed lines indicate this interaction between the two ensembles.

III. METHODOLOGY

The idea is to initially spin squeeze the ensembles individually and then couple them to create entanglement (see Fig. 1 for a conceptual illustration). The details of the process are as follows. Each ensemble is first initialized as a coherent spin state by collectively aligning the spins along the x axis, i.e., $|\psi\rangle = [\frac{1}{\sqrt{2}}(|-1\rangle + |+1\rangle)]^{\otimes N}$. Afterward, the time evolution of the ensemble state is computationally simulated according to the master equation with the spin squeezing Hamiltonian (4) and the appropriate decoherence, for some squeezing time t_s. Next, the two ensembles are coupled and the time evolution of the composite two-ensemble state is simulated, again using the master equation with either entanglement Hamiltonian (9) or (13) and the appropriate decoherence, for some amount of entanglement time t_e. Finally, the degree of entanglement is quantified using the measure of logarithmic negativity [58,59] over the duration of entanglement time t_e. The logarithmic negativity has the physical meaning of the upper bound to entanglement distillation [60].

In the phonon-photon and phonon-phonon scenarios, the number of spins N involved is relatively small, so it is possible to perform a more straightforward simulation of the density operator. In the photon-photon scenario, however, the number of spins involved is much larger and the direct simulation of the density operator is not practically feasible. Therefore, different approaches are required depending on whether the number of spins N is small or very large.

A. Small N under the phonon-photon and phonon-phonon scenarios

Since each spin state is a two-level quantum system, the full Hilbert space of an ensemble has dimension 2^N. Since the size grows exponentially with N, this can make numerical computation impractical even for relatively small N. To mitigate this issue, the ensemble is expressed in the Dicke state basis [38] instead. In this basis, the dimension of the collective spin state is reduced to $N+1$ (for details on this basis, see Appendix A).

With this, the density matrix ρ of the two-ensemble composite state has $(N+1)^4$ entries. The numerical computation can be made more efficient by making use of the fact that the density matrix is Hermitian $\rho^\dagger = \rho$. For this reason, it is possible to store and compute only the entries that belong in either the upper or lower triangular part of the matrix.

Additionally, if we assume identical ensembles, then the two-ensemble composite state is symmetric under exchange between the two ensembles. More precisely, the entries satisfy $\rho_{f(i,k),f(j,l)} = \rho_{f(k,i),f(l,j)}$, where $f(\alpha,\beta) = (N+1)(\alpha-1)+\beta$. This will further reduce the number of entries in ρ that need to be stored and computed to have the full information of the system. Finally, the logarithmic negativity of density operator ρ is computed according to

$$E_N = \ln \|\rho^{\Gamma_A}\|_1, \tag{19}$$

where $\|\rho^{\Gamma_A}\|_1$ is the trace norm of ρ^{Γ_A} ($\|K\|_1 = \mathrm{Tr}\sqrt{K^\dagger K}$) and Γ_A denotes the partial transpose operation on ρ with respect to subsystem A, which can be either ensemble 1 or ensemble 2.

B. Large-N limit under the photon-photon scenario

In the limit of large N, the spin operators can be mapped to boson operators using the Holstein-Primakoff transformation [61]. The transformations are written as $J_+ = \sqrt{N-a^\dagger a}a$, $J_- = a^\dagger\sqrt{N-a^\dagger a}$, and $J_z = \frac{N}{2} - a^\dagger a$. Furthermore, if $\langle J_z\rangle \approx \frac{N}{2}$, then we may keep only terms up to second order in boson operators in the master equation, ignoring the much smaller contribution from the higher-order terms. Up to second order in boson operators, $J_+ \approx \sqrt{N}a$, $J_- \approx \sqrt{N}a^\dagger$, $J_x = (J_+ + J_-)/2 \approx \sqrt{N}(a+a^\dagger)/2 = \sqrt{N/2}\hat{x}$, and $J_y = (J_+ - J_-)/2i \approx \sqrt{N}(a-a^\dagger)/2i = \sqrt{N/2}\hat{p}$, where $\hat{x} = (a+a^\dagger)/\sqrt{2}$ and $\hat{p} = (a-a^\dagger)/\sqrt{2}i$ are quadrature operators.

With the mapping to boson operators, the spin systems are effectively treated as continuous-variable systems. For a continuous-variable system, it is convenient to represent the state using the Wigner characteristic function $W(\chi) = \mathrm{Tr}[\rho\exp(\chi a^\dagger - \chi^* a)]$ [62]. This can also be equivalently expressed in terms of the quadrature operators $\hat{x} = (a+a^\dagger)/\sqrt{2}$ and $\hat{p} = (a-a^\dagger)/\sqrt{2}i$, that is, $W(u,v) = \mathrm{Tr}[\rho\exp(u\hat{x} + v\hat{p})]$, where $u = (\chi-\chi^*)/\sqrt{2}$ and $v = (\chi+\chi^*)/\sqrt{2}\mathrm{i}$ are independent parameters. For bipartite continuous-variable states, the Wigner characteristic function can be expressed

as $W(\mathbf{V}) = \mathrm{Tr}[\rho \exp(\mathbf{V}^{\mathrm{T}}\hat{\mathbf{R}})]$, where $\mathbf{V} = (u_1, v_1, u_2, v_2)^{\mathrm{T}}$ and $\hat{\mathbf{R}} = (\hat{x}_1, \hat{p}_1, \hat{x}_2, \hat{p}_2)^{\mathrm{T}}$ are in vector form.

The master equation for ρ can be transformed into a partial differential equation for the Wigner characteristic function using a slightly modified operator correspondence

$$\rho\hat{x}_j \to \left(\frac{\partial}{\partial u_j} + i\frac{v_j}{2}\right)W(\mathbf{V}), \tag{20a}$$

$$\hat{x}_j\rho \to \left(\frac{\partial}{\partial u_j} - i\frac{v_j}{2}\right)W(\mathbf{V}), \tag{20b}$$

$$\hat{p}_j\rho \to \left(\frac{\partial}{\partial v_j} + i\frac{u_j}{2}\right)W(\mathbf{V}), \tag{20c}$$

$$\rho\hat{p}_j \to \left(\frac{\partial}{\partial v_j} - i\frac{u_j}{2}\right)W(\mathbf{V}), \tag{20d}$$

where the index $j = \{1, 2\}$ denotes ensemble 1 or ensemble 2. (For the details on how this operator correspondence is obtained, refer to Appendix C). This correspondence can be extended to the action of the second-order quadrature operators on ρ. For example,

$$\rho\hat{x}_j\hat{p}_k \to \left(\frac{\partial}{\partial v_k} - i\frac{u_k}{2}\right)\left(\frac{\partial}{\partial u_j} + i\frac{v_j}{2}\right)W(\mathbf{V}). \tag{21}$$

With the ensembles initialized as coherent spin states and the master equation having only terms up to second order in boson operators, the systems take the form of a special class of continuous-variable states called Gaussian states [63–65]. For Gaussian states, the Wigner characteristic function $W(\mathbf{V}) = \mathrm{Tr}[\rho \exp(\mathbf{V}^{\mathrm{T}}\hat{\mathbf{R}})]$ is a Gaussian function. Namely,

$$W(\mathbf{V}) = \exp\left(\tfrac{1}{2}\mathbf{V}^{\mathrm{T}}\sigma\mathbf{V} + \mathbf{V}^{\mathrm{T}}\langle\hat{\mathbf{R}}\rangle\right), \tag{22}$$

where σ is the covariance matrix and the expectation value $\langle\hat{\mathbf{R}}\rangle = (\langle\hat{x}_1\rangle, \langle\hat{p}_1\rangle, \langle\hat{x}_2\rangle, \langle\hat{p}_2\rangle)^{\mathrm{T}}$ for bipartite states. The term $\mathbf{V}^{\mathrm{T}}\langle\hat{\mathbf{R}}\rangle$ does not contain any information about entanglement as it only contains information about position in the phase space. Therefore, the full information about the entanglement is encoded within the correlation in the covariance matrix σ. Its elements are defined as the covariance

$$\sigma_{ij} = \tfrac{1}{2}\langle\hat{R}_i\hat{R}_j + \hat{R}_j\hat{R}_i\rangle - \langle\hat{R}_i\rangle\langle\hat{R}_j\rangle \tag{23}$$

and they obey $\sigma_{ij} = \sigma_{ji}$, or $\sigma^{\mathrm{T}} = \sigma$. The logarithmic negativity can be obtained from the covariance matrix σ according to

$$E_N = \max\left\{0, -\tfrac{1}{2}\ln\eta\right\}, \tag{24}$$

with

$$\eta = 2(\zeta - \sqrt{\zeta^2 - 4\det\sigma}), \tag{25a}$$

$$\zeta = \det B + \det D - 2\det C, \tag{25b}$$

$$\sigma = \begin{pmatrix} B & C \\ C^{\mathrm{T}} & D \end{pmatrix}, \tag{25c}$$

where B, C, and D are 2×2 submatrices of σ.

The process of obtaining the time evolution of the covariance matrix $\dot{\sigma}$ is described as follows. First, the time evolution of the Wigner characteristic function is obtained from the master equation by applying the operator correspondence (20) in conjunction with the Gaussian Wigner characteristic function in (22). In addition, this time evolution obtained from operator correspondence must also follow the time-derivative form of (22), that is,

$$\frac{\partial}{\partial t}W(\mathbf{V}, t) = \left(\frac{1}{2}\mathbf{V}^{\mathrm{T}}\dot{\sigma}\mathbf{V} + \mathbf{V}^{\mathrm{T}}\frac{d}{dt}\langle\hat{\mathbf{R}}\rangle\right)W(\mathbf{V}, t). \tag{26}$$

Finally, the time evolution of each entry of σ is obtained by simply matching the parameters in $\mathbf{V}$ between this form and the one obtained by operator correspondence.

For the purpose of illustration, the process is presented here for the time evolution of σ corresponding to the master equation for the squeezing Hamiltonian in (4) and its decoherence in (16), with $F = J_-$. The time evolution of the Wigner characteristic function and covariance matrix elements for the entanglement Hamiltonians (9) and (13) with their respective decoherence are given in Appendix D.

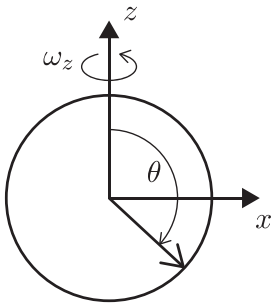

FIG. 2. Diagram of the mean spin direction with polar angle θ and rotation rate ω_z with respect to the z axis.

1. Illustration of the time evolution for the squeezing Hamiltonian

The master equation corresponding to the squeezing Hamiltonian is given by

$$\dot{\rho} = \frac{g_c^2}{\Delta}\Big[i\big(J_z^2\rho - \rho J_z^2\big) + \frac{\kappa}{\Delta}\left(J_-\rho J_+ - \frac{1}{2}(J_+J_-\rho + \rho J_+J_-)\right)\Big]. \tag{27}$$

Note that the $\mathbf{J}^2$ term disappears. This is related to the fact that the spin operators that appear in the time evolution due to the Hamiltonian and decoherence are all collective ensemble spin operators. Because collective spin operators cannot change the magnitude of the collective spin vector for the ensemble, the $\mathbf{J}^2$ term is effectively a constant. The linear J_z terms are dropped since they only cause rotation about the z axis. This will not affect the squeezing or entanglement dynamics of the system.

Let us assume that the mean spin direction lies on the xz plane. Let θ be the polar angle (measured from the z axis; see Fig. 2) of the mean spin direction in the collective Bloch sphere. So in the initial alignment of the coherent spin state on the x axis, $\theta = \pi/2$. In order to fulfill the requirement that $\langle J_z\rangle \approx \frac{N}{2}$, coordinate transformation must be performed so that the mean spin direction points towards the z axis.

This can be achieved by applying the transformation

$$J_x \to J_x \cos\theta + J_z \sin\theta, \tag{28a}$$

$$J_y \to J_y, \tag{28b}$$

$$J_z \to J_z \cos\theta - J_x \sin\theta. \tag{28c}$$

Afterward, the Holstein-Primakoff transformation can be applied to map the spin operators to boson operators. Applying these transformations to the terms in (27), up to second order in boson operators, yields

$$J_z^2 \to \frac{N}{2}\left\{\left[\left(\frac{N}{2}+1\right) - (\hat{x}^2+\hat{p}^2)\right]\cos^2\theta + \hat{x}^2\sin^2\theta - \sqrt{2N}\hat{x}\sin\theta\cos\theta\right\}, \tag{29}$$

$$J_+J_- \to \frac{N}{2}\left\{\left[\left(\frac{N}{2}+1\right) - (\hat{x}^2+\hat{p}^2)\right]\sin^2\theta + \hat{p}^2 + \hat{x}^2\cos^2\theta + \sqrt{2N}\hat{x}\sin\theta\cos\theta + \cos\theta\right\}, \tag{30}$$

and

$$J_-\rho J_+ \to \frac{N}{2}\left\{\left[\left(\frac{N}{2}+1\right)\rho - \frac{1}{2}(\hat{x}^2+\hat{p}^2)\rho - \frac{1}{2}\rho(\hat{x}^2+\hat{p}^2)\right]\sin^2\theta + \hat{p}\rho\hat{p} + \hat{x}\rho\hat{x}\cos^2\theta + \sqrt{\frac{N}{2}}(\hat{x}\rho+\rho\hat{x})\sin\theta\cos\theta - i\left[\sqrt{\frac{N}{2}}(\hat{p}\rho-\rho\hat{p})\sin\theta + (\hat{p}\rho\hat{x}-\hat{x}\rho\hat{p})\cos\theta\right]\right\}, \tag{31}$$

where terms with a coefficient much less than N have been ignored since they are negligible compared to the other terms. Finally, applying the operator correspondence (20) gives the time evolution for the Wigner characteristic function

$$\dot{W}(u,v,t_s) = \frac{Ng_c^2}{\Delta}\left\{\left[\cos^2\theta\left(u\frac{\partial}{\partial v} - v\frac{\partial}{\partial u}\right) + \sin^2\theta\, v\frac{\partial}{\partial u} - \sqrt{\frac{N}{2}}\sin\theta\cos\theta\, v\right] + \frac{\kappa}{2\Delta}\left[\frac{1}{2}u^2 + \cos^2\theta\frac{1}{2}v^2 + \sqrt{\frac{N}{2}}\sin\theta u + \cos\theta\left(u\frac{\partial}{\partial u} + v\frac{\partial}{\partial v}\right)\right]\right\}W(u,v,t_s). \tag{32}$$

2. Rotation

We have assumed earlier that the mean spin direction lies on the xz plane. This may not always be true since the spin ensemble may rotate about the z axis. In order for it to be valid at all times, it is necessary to move into a rotating frame of reference which follows the rotation of the mean spin direction about the z axis. In this frame, the mean spin direction always lies on the xz plane. Moving into this frame is done by putting the counterrotation term $-\omega_z J_z$ in the Hamiltonian. In the case of two ensembles, it is done by putting $-\omega_z(J_1^z + J_2^z)$ in the Hamiltonian, which corresponds to a rotating frame with a common rotation rate ω_z. Note that although the linear J_z terms have been dropped from the master equation earlier, the other terms in the master equation may still cause additional rotation about the z axis. Putting in $-\omega_z J_z$ accounts for this fact. Alternatively, it is also possible to keep the linear J_z terms from the master equation at the beginning and account for everything later with $-\omega_z J_z$. However, dropping the terms early from the master equation makes the analysis simpler due to dealing with fewer terms. Note that the Hamiltonians and master equations due to decoherence in our analysis are all invariant under angular displacement about the z axis (or azimuthal angle in the Bloch sphere).

In addition to rotation about the z axis, the spin ensemble may also rotate in the polar direction, causing the polar angle θ to change. Because the mean spin direction is required to always point towards the z axis after the coordinate transformation (i.e., it stays in place), it is necessary that the rotating frame of reference also follows the rotation of the mean spin direction along the polar direction. This is done by putting the additional counterrotation term $-\dot{\theta}J_y$ in the Hamiltonian. So finally the rotating frame of reference essentially follows the rotation of the spin ensemble in both the azimuthal (associated with ω_z) and polar (associated with $\dot{\theta}$) angular directions. In this rotating frame of reference, the mean spin direction points towards the z axis and remains stationary. The task here is to determine the appropriate values for ω_z and $\dot{\theta}$ for this rotating frame of reference.

If the considerations for the rotating frame of reference above are not taken into account, the consequence is that the continuous rotation of the spin ensemble causes the mean spin direction to move around and deviate from the z axis in the transformed coordinate system. For the continuous-variable state, this causes the expectation values $\langle\hat{x}\rangle$ and $\langle\hat{p}\rangle$ to move away from zero, or the center or origin of the phase space. This is also indicated by nonzero $\frac{d}{dt_s}\langle\hat{x}\rangle$ and $\frac{d}{dt_s}\langle\hat{p}\rangle$.

Let us consider for a moment the Hamiltonians for rotation $\dot{\theta}J_y$ and $\omega_z J_z$. Applying the coordinate transformation (28), Holstein-Primakoff transformation, and operator correspondence (20) consecutively yields

$$\dot{W}(u,v,t_s) = \dot{\theta}\sqrt{\frac{N}{2}}uW(u,v,t_s) \tag{33}$$

for $\dot{\rho}_\theta = -i\dot{\theta}[J_y,\rho]$ and

$$\dot{W}(u,v,t_s) = \omega_z\left[\cos\theta\left(v\frac{\partial}{\partial u} - u\frac{\partial}{\partial v}\right) + \sqrt{\frac{N}{2}}\sin\theta\, v\right]W(u,v,t_s) \tag{34}$$

for $\dot{\rho}_z = -i\omega_z[J_z,\rho]$. The next step is to match the parameters u and v with Eq. (26). Expanding this equation for the 2×2 covariance matrix for a single continuous-variable state

yields

$$\dot{W}(u,v,t_s) = \left(\frac{1}{2}[\dot{\sigma}_{11}u^2 + (\dot{\sigma}_{12}+\dot{\sigma}_{21})uv + \dot{\sigma}_{22}v^2] + u\frac{d}{dt_s}\langle\hat{x}\rangle + v\frac{d}{dt_s}\langle\hat{p}\rangle\right)W(u,v,t_s). \quad (35)$$

It is straightforward to match the parameters in (33) with this equation, which gives

$$\frac{d}{dt_s}\langle\hat{x}\rangle = \dot{\theta}\sqrt{\frac{N}{2}}, \quad (36a)$$

$$\frac{d}{dt_s}\langle\hat{p}\rangle = 0 \quad (36b)$$

for $H = \dot{\theta}J_y$.

Equation (34) cannot be directly compared with Eq. (35) due to the derivative terms with respect to u and v. It is necessary to apply the Gaussian form in (22) to (34) first. Writing down (22) for the 2×2 covariance matrix for a single continuous-variable state gives

$$W(u,v,t_s) = \exp\left\{\tfrac{1}{2}[\sigma_{11}u^2 + (\sigma_{12}+\sigma_{21})uv + \sigma_{22}v^2] + u\langle\hat{x}\rangle + v\langle\hat{p}\rangle\right\}. \quad (37)$$

Inserting this into (34) gives

$$\dot{W}(u,v,t_s) = \omega_z\Bigg[\cos\theta\left(\frac{1}{2}(\sigma_{12}+\sigma_{21})(v^2-u^2) + (\sigma_{11}-\sigma_{22})uv\right) - u\langle\hat{p}\rangle\cos\theta + v\left(\sqrt{\frac{N}{2}}\sin\theta + \langle\hat{x}\rangle\cos\theta\right)\Bigg]W(u,v,t_s). \quad (38)$$

Finally, $\frac{d}{dt_s}\langle\hat{x}\rangle$ and $\frac{d}{dt_s}\langle\hat{p}\rangle$ are obtained from (38) by matching parameters with (35), which yields

$$\frac{d}{dt_s}\langle\hat{x}\rangle = -\omega_z\langle\hat{p}\rangle\cos\theta, \quad (39a)$$

$$\frac{d}{dt_s}\langle\hat{p}\rangle = \omega_z\left(\sqrt{\frac{N}{2}}\sin\theta + \langle\hat{x}\rangle\cos\theta\right) \quad (39b)$$

for $H = \omega_z J_z$.

In the rotating frame of reference, the mean spin direction stays along the z axis and the expectation values $\langle\hat{x}\rangle$ and $\langle\hat{p}\rangle$ remain zero in the phase space of the continuous-variable state. Moving into the rotating frame is done by putting $-\omega_z J_z$ and $-\dot{\theta}J_y$ in the Hamiltonian to offset the effects of rotation. The appropriate values of ω_z and $\dot{\theta}$ for Eq. (32) so that $\frac{d}{dt_s}\langle\hat{x}\rangle = 0$ and $\frac{d}{dt_s}\langle\hat{p}\rangle = 0$ are

$$\omega_z = -\frac{Ng_c^2}{\Delta}\cos\theta, \qquad \dot{\theta} = \frac{\kappa N g_c^2}{2\Delta^2}\sin\theta. \quad (40)$$

In the frame of the original coordinate system associated with master Eq. (27), ω_z denotes the rate of rotation of the mean spin direction about the z axis and $\dot{\theta}$ denotes the rate of change of its polar angle. In the rotating frame of reference, time evolution for the Wigner characteristic function is

$$\dot{W}(u,v,t_s) = \frac{Ng_c^2}{\Delta}\left\{\sin^2\theta\, v\frac{\partial}{\partial u} + \frac{\kappa}{2\Delta}\left[\frac{1}{2}u^2 + \cos^2\theta\frac{1}{2}v^2 + \cos\theta\left(u\frac{\partial}{\partial u} + v\frac{\partial}{\partial v}\right)\right]\right\}W(u,v,t_s). \quad (41)$$

3. *Time evolution of the covariance matrix*

Applying the Gaussian form in (37) to (41) yields

$$\dot{W}(u,v,t_s) = \frac{Ng_c^2}{\Delta}\Bigg[\sin^2\theta\left(\sigma_{11}uv + \frac{1}{2}(\sigma_{12}+\sigma_{21})v^2\right) + \frac{\kappa}{2\Delta}\left(\frac{1}{2}u^2 + \cos^2\theta\frac{1}{2}v^2 + \cos\theta[\sigma_{11}u^2 + (\sigma_{12}+\sigma_{21})uv + \sigma_{22}v^2]\right)\Bigg]W(u,v,t_s). \quad (42)$$

The next step is to match the parameters u and v with Eq. (35). Note that $\frac{d}{dt_s}\langle\hat{x}\rangle = 0$ and $\frac{d}{dt_s}\langle\hat{p}\rangle = 0$ in the rotating frame of reference, as discussed previously. Matching the rest of the parameters in the two equations above yields

$$\dot{\sigma}_{11} = \frac{\kappa N g_c^2}{2\Delta^2}(1 + 2\sigma_{11}\cos\theta), \quad (43a)$$

$$\dot{\sigma}_{22} = \frac{Ng_c^2}{\Delta}\left(2\sigma_{12}\sin^2\theta + \frac{\kappa}{2\Delta}(\cos^2\theta + 2\sigma_{22}\cos\theta)\right), \quad (43b)$$

$$\dot{\sigma}_{21} = \dot{\sigma}_{12} = \frac{Ng_c^2}{\Delta}\left(\sigma_{11}\sin^2\theta + \frac{\kappa}{\Delta}\sigma_{12}\cos\theta\right), \quad (43c)$$

where the fact that $\sigma_{21} = \sigma_{12}$ has been used. Together with $\dot{\theta}$ given in (40) and the initial conditions $\theta(t_s = 0) = \pi/2$ and $\sigma(t_s = 0) = \frac{1}{2}I_2$, where I_2 is the 2×2 identity matrix, the time evolution of covariance matrix $\dot{\sigma}$ can be numerically computed.

IV. RESULTS AND DISCUSSION

A. Phonon-photon scenario

Here the initial squeezing of individual ensembles is mediated by phonons and the entanglement of two ensembles is mediated by photons. The numbers of spins considered in this scenario are $N = 50$ and 100 in a single ensemble, and so the small-N approach in Sec. III A is used. In the calculation, the parameters we consider are $\bar{n}_{th} = 1$, corresponding to $T \sim 70$ mK for $\omega_m/2\pi \sim 1$ GHz, and a fixed decoherence factor $\gamma/\Delta = 0.01$.

First, the time evolution of logarithmic negativity E_N for the entanglement Hamiltonian $H_{\text{ent},-}$ [Eq. (9)], implementing several different squeezing times, is shown in Fig. 3 for a number of spins $N = 50$ in a single ensemble with a range of photon decoherence factors $\kappa/\Delta = 0$, 0.001, 0.01, and 0.1. Additionally, Fig. 3(a) also shows the results for $N = 100$ and $\kappa/\Delta = 0.01$. The squeezing time is indicated by $t_s' = (Ng_m^2/\Delta)t_s$, which is dimensionless. Along with this scaled squeezing time, we also compute the squeezing parameter ξ_S^2 [13,18] to quantify the amount of squeezing

$$\xi_S^2 = \frac{4(\Delta J_\perp)^2_{\min}}{N}, \quad (44)$$

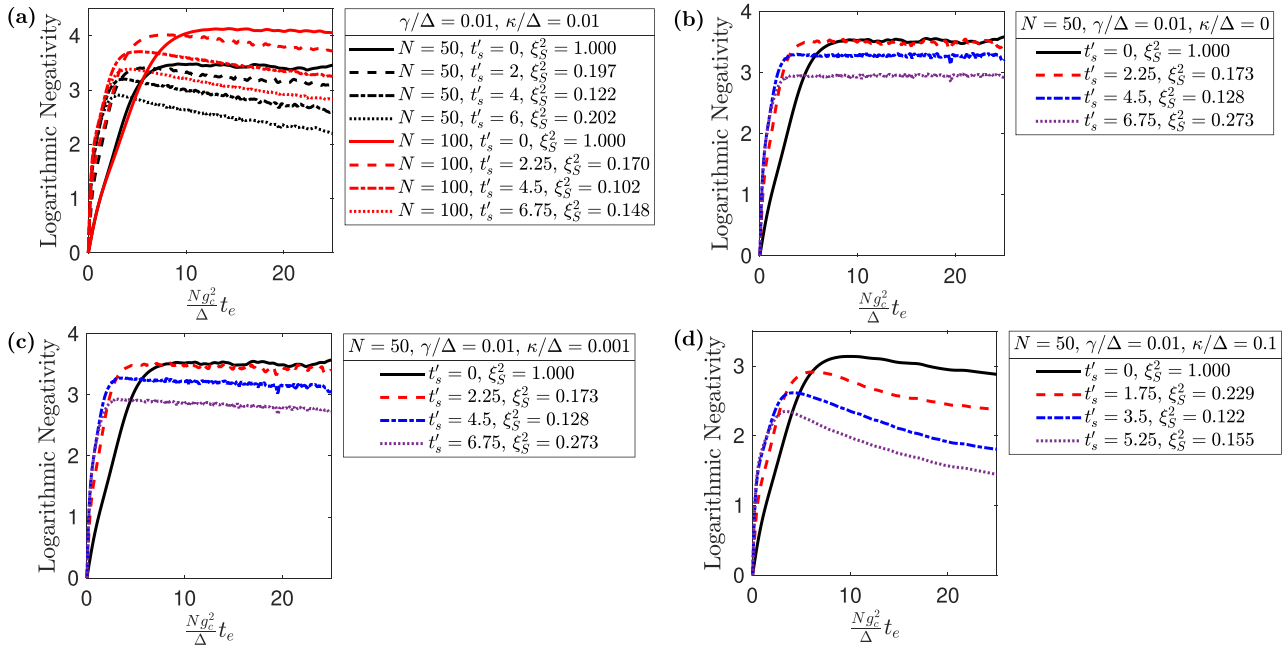

FIG. 3. Time evolution of logarithmic negativity E_N against dimensionless entanglement time $(Ng_c^2/\Delta)t_e$ for $\gamma/\Delta = 0.01$ with different dimensionless squeezing times $t_s' = (Ng_m^2/\Delta)t_s$ in the phonon-photon scenario for the entanglement Hamiltonian $H_{\text{ent},-}$ for (a) $N = 50$ and 100 and $\kappa/\Delta = 0.01$, (b) $N = 50$ and $\kappa/\Delta = 0$, (c) $N = 50$ and $\kappa/\Delta = 0.001$, and (d) $N = 50$ and $\kappa/\Delta = 0.1$.

where $(\Delta J_\perp)^2_{\text{min}}$ is the variance of the spin measurement, minimized over all directions perpendicular to the mean spin direction. For the coherent spin state $\xi_S^2 = 1$, while for the squeezed state $\xi_S^2 < 1$.

From the results displayed in the figure, it can be seen that implementation of initial squeezing improves E_N, but only initially. Over a longer period of time, there is no distinctive improvement from initial squeezing. This will be further discussed later. Also, having more spins in the ensembles increases E_N.

Next, the time evolution of E_N for entanglement Hamiltonian $H_{\text{ent},+}$ [Eq. (13)] is shown in Fig. 4. Figure 4(a) displays the results for $N = 50$ and 100 and $\kappa/\Delta = 0.01$. Figure 4(b) displays the results for $N = 50$ with a range of $\kappa/\Delta = 0$, 0.001, 0.01, and 0.1. Instead of using several different values of dimensionless squeezing times t_s', a single value of t_s' that approximately gives the optimal E_N is chosen. Note that optimal entanglement may not necessarily occur at optimal squeezing indicated by a minimum ξ_S^2. Furthermore, for a given value of ξ_S^2, there are two points in time during initial squeezing that this may occur. Therefore, the squeezing parameter ξ_S^2 and squeezing time t_s' must be taken together to characterize the initial squeezing that gives the optimal entanglement.

The results show that implementing initial squeezing improves E_N overall. Combined with having more spins in the ensembles further improves E_N slightly. The fact that initial squeezing here enhances entanglement stands in contrast to the previous results for entanglement Hamiltonian $H_{\text{ent},-}$. This observation will be further discussed later.

Let us now discuss the estimation of the entanglement timescale in the results. Assuming that $\omega_c/2\pi \sim 1$ GHz and $Q = 10^3$, we get $\kappa/2\pi = \omega_c/2\pi Q \sim 1$ GHz. This corresponds to $\Delta/2\pi = 100$ MHz for $\kappa/\Delta = 0.01$. With the coupling strength of a single NV center of $g_c/2\pi \sim 10$ Hz, for $N = 100$, the dimensionless entanglement time of $t_e' = 25$

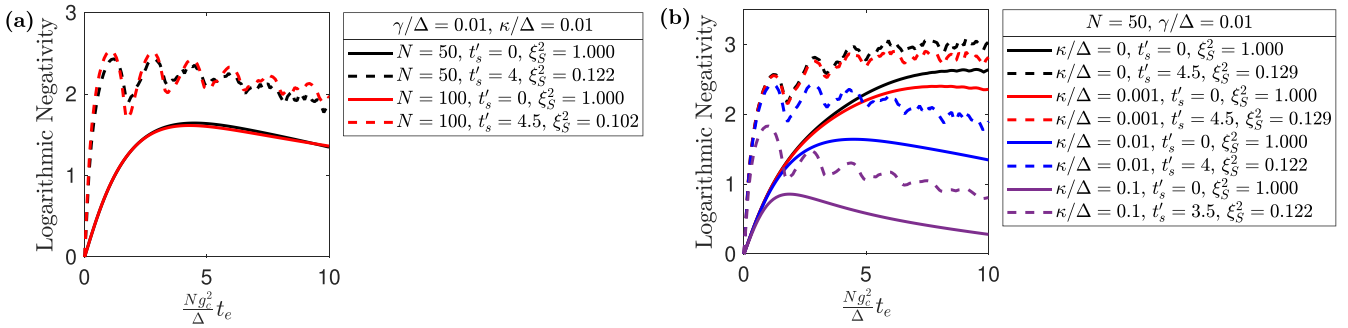

FIG. 4. Time evolution of logarithmic negativity E_N against dimensionless entanglement time $(Ng_c^2/\Delta)t_e$ for $\gamma/\Delta = 0.01$ in the phonon-photon scenario for the entanglement Hamiltonian $H_{\text{ent},+}$ for (a) $N = 50$ and 100 and $\kappa/\Delta = 0.01$ and (b) $N = 50$ and $\kappa/\Delta = 0$, 0.001, 0.01, and 0.1.

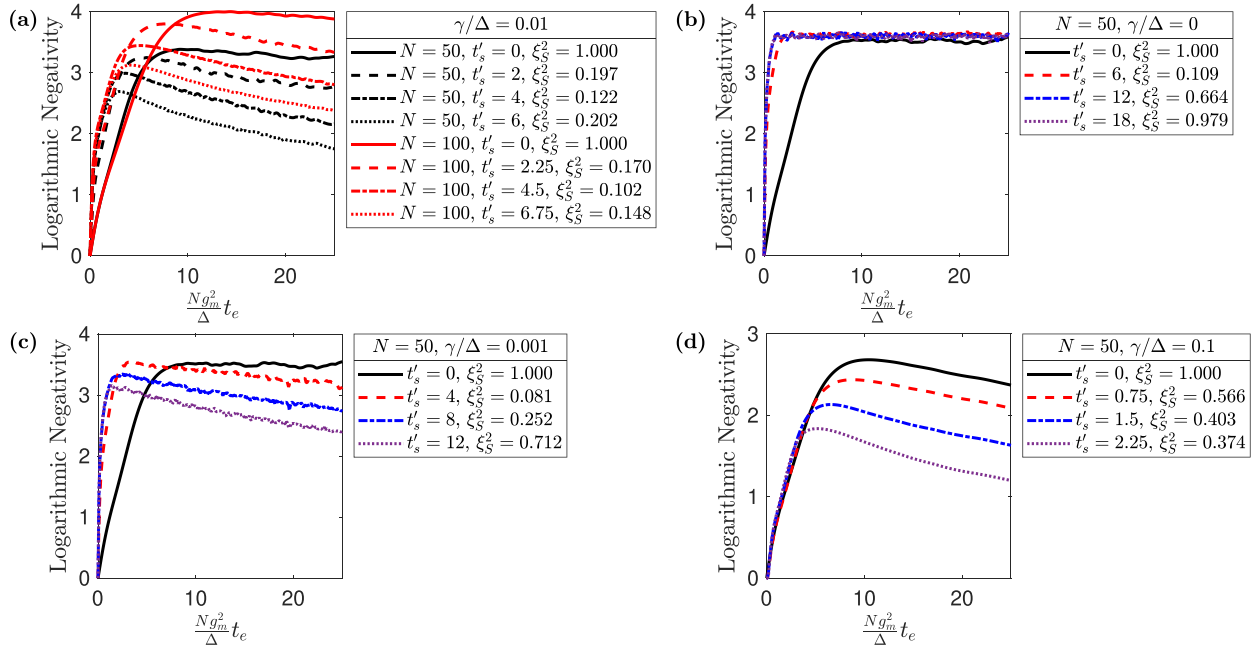

FIG. 5. Time evolution of logarithmic negativity E_N against dimensionless entanglement time $(Ng_m^2/\Delta)t_e$ with different dimensionless squeezing times $t'_s = (Ng_m^2/\Delta)t_s$ in the phonon-phonon scenario for the entanglement Hamiltonian $H_{\text{ent},-}$ for (a) $N = 50$ and 100 and $\gamma/\Delta = 0.01$, (b) $N = 50$ and $\gamma/\Delta = 0$, (c) $N = 50$ and $\gamma/\Delta = 0.001$, and (d) $N = 50$ and $\gamma/\Delta = 0.1$.

corresponds to $t_e \approx 4 \times 10^4$ s. This timescale is clearly far above the coherence times T_1 and T_2 of the NV center. The spin-relaxation effects associated with T_1 and T_2 cannot be ignored anymore and they would dominate much of the dynamics of the system throughout this timescale to eliminate entanglement. Thus, the results shown here would be valid only for a very short initial time period. The entanglement timescale can be shortened by lowering the detuning Δ, but unless the quality factor Q is also improved, dissipative decoherence would have a more dominant effect. This represents the limitation of this scenario due to the weak coupling of the individual NV center in the optical resonator system, which necessitates consideration of the other scenarios.

B. Phonon-phonon scenario

Here, both the initial squeezing of individual ensembles and the entanglement of two ensembles are mediated by phonons. The numbers of spins considered in this scenario are $N = 50$ and 100 in a single ensemble, and so the small-N approach in Sec. III A is used. Instead of fixing the decoherence factor γ/Δ to a single value, choices of different values are used in the calculation.

The time evolution of logarithmic negativity E_N for the entanglement Hamiltonian $H_{\text{ent},-}$ is shown in Fig. 5. In general, the results have characteristics similar to the phonon-photon case. Implementation of initial squeezing improves E_N only initially, but this improvement does not continue over a longer period of time. Increasing the number of spins in the ensembles also increases E_N.

The time evolution of E_N for the entanglement Hamiltonian $H_{\text{ent},+}$ is shown in Fig. 6 for optimal dimensionless squeezing time t'_s. Again, the results are similar to the phonon-photon scenario. Implementation of initial squeezing improves E_N in general. Also, initial squeezing in combination with more spins in the ensembles slightly improves E_N.

In general, at the beginning, initial squeezing enhances entanglement for both entanglement Hamiltonians $H_{\text{ent},+}$ and $H_{\text{ent},-}$. While this enhancement continues for $H_{\text{ent},+}$ to a longer period of time, it does not continue for $H_{\text{ent},-}$. Looking at Fig. 5(b), even without decoherence, initial squeezing does not increase logarithmic negativity E_N further at later time. In fact, E_N saturates at about the same value, with or without initial squeezing, which suggests that there is an upper bound for E_N. It has been shown in a previous study [66] that there exists a universal dynamical bound on entanglement. It was found that if entanglement is created from two unentangled subsystems by a dynamical process described by some generic entanglement Hamiltonian, then there is a universal bound for the entropy of entanglement.

To show that this bound on entanglement is achieved, it is necessary to compare it with the entanglement entropy from our results. The dynamical bound for entropy of entanglement for two subsystems of equal size dimension is given by $S_b \sim \ln(0.6D)$ [66], where D is the Hilbert space dimension of a subsystem. In our case, since it is possible to reduce the Hilbert space dimension of a spin ensemble to $D = N + 1$, the bound for entanglement entropy is estimated to be $S_b \sim \ln[0.6(N + 1)]$. It is important to note that this bound is a *statistical* bound, meaning that it is possible for entanglement entropy to fluctuate around this bound at saturation, but *on average* it does not exceed this bound. Figure 7 shows the entropy of entanglement for both $H_{\text{ent},-}$ and $H_{\text{ent},+}$ for $N = 50$ and 100. Purely without decoherence, the plots for both the phonon-photon and phonon-phonon scenarios are identical. It can be seen in the figure that, for both $H_{\text{ent},-}$ and $H_{\text{ent},+}$, saturation with initial squeezing occurs and fluctuates around the estimated bound. Without initial squeezing, entropy for

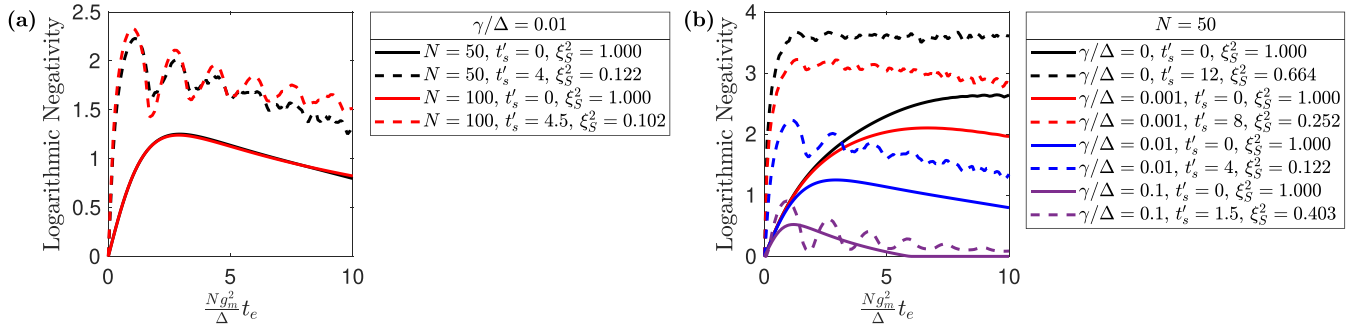

FIG. 6. Time evolution of logarithmic negativity E_N against dimensionless entanglement time $(Ng_m^2/\Delta)t_e$ in the phonon-phonon scenario for the entanglement Hamiltonian $H_{\text{ent},+}$ for (a) $N = 50$ and 100 and $\gamma/\Delta = 0.01$ and (b) $N = 50$ and $\gamma/\Delta = 0$, 0.001, 0.01, and 0.1.

$H_{\text{ent},-}$ saturates near the bound, while for $H_{\text{ent},+}$ it does not approach this bound.

Saturation of entanglement entropy at or near the bound implies that logarithmic negativity E_N has also reached its own corresponding bound by extension. Similarly, if entanglement entropy does not reach the bound, E_N also does not reach its corresponding bound. In fact, the bound for E_N appears to be very close to that for the entropy of entanglement, i.e., $\sim \ln[0.6(N+1)]$, as can be seen in Figs. 5(b) and 6(b). Because E_N is already able to approach this bound without initial squeezing for $H_{\text{ent},-}$, performing initial squeezing does not push E_N much higher. For $H_{\text{ent},+}$, on the other hand, E_N does not yet approach this bound without initial squeezing and therefore application of initial squeezing can increase E_N further. In Fig. 6(b) we can also see that without decoherence, E_N with initial squeezing for $H_{\text{ent},+}$ saturates at precisely the same bound as $H_{\text{ent},-}$. Note that for the phonon-photon scenario in Fig. 3(b), E_N saturates at different values because we take into account decoherence during initial squeezing. The longer initial squeezing with decoherence is applied, the lower the saturation value for E_N is.

The existence of the universal dynamical bound discussed above causes initial squeezing to induce no further improvement towards E_N at later time for $H_{\text{ent},-}$, even without decoherence. Additionally, the presence of decoherence makes the curves for E_N slope downward eventually with time, causing E_N with initial squeezing to be lower than that with no initial squeezing at later time. For $H_{\text{ent},+}$ though, this is not the case: At later time, the implementation of initial squeezing still improves E_N compared to that without initial squeezing. This difference in the effect of decoherence can be explained through the analysis in the large-N limit, which will be discussed later.

As mentioned previously, the phonon-phonon scenario may be considered to improve the coupling strength of entanglement, which should make the response time faster. Taking the same assumption as the phonon-photon scenario for the other experimental parameters, $\omega_m/2\pi \sim 1$ GHz, $Q = 10^5$, and $\gamma/\Delta = 0.01$, we obtain $\Delta/2\pi = 1$ MHz. With a coupling strength of $g_m/2\pi \sim 1$ kHz, for $N = 100$, the dimensionless entanglement time of $t_e' = 25$ corresponds to $t_e \approx 0.04$ s, which is considerably shorter than $T_2 \sim 0.6$ s in [3]. This means that the main entanglement dynamics occurs at a shorter timescale before the individual spin-relaxation effects become dominant.

C. Photon-photon scenario

In this scenario, both the initial squeezing of individual ensembles and the entanglement of two ensembles are mediated by photons. The number of spins considered in this scenario is $N \sim 10^{12}$ in a single ensemble, and so the large-N limit approach in Sec. III B is used. For initial squeezing in this case, the squeezing parameter in terms of the covariance matrix elements for a single ensemble is given by

$$\xi_S^2 = \sigma_{11} + \sigma_{22} - \sqrt{(\sigma_{11} - \sigma_{22})^2 + 4\sigma_{12}^2}. \tag{45}$$

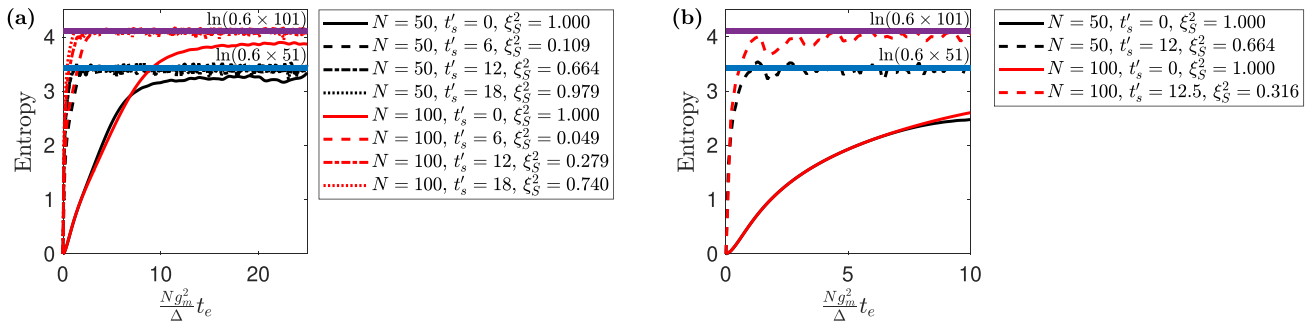

FIG. 7. Time evolution of entanglement entropy against dimensionless entanglement time $(Ng_m^2/\Delta)t_e$ in both the phonon-photon and phonon-phonon scenarios with $N = 50$ and 100 under no decoherence for the entanglement Hamiltonians (a) $H_{\text{ent},-}$ and (b) $H_{\text{ent},+}$. Horizontal solid lines represent the bounds $\ln(0.6 \times 51)$ for $N = 50$ and $\ln(0.6 \times 101)$ for $N = 100$.

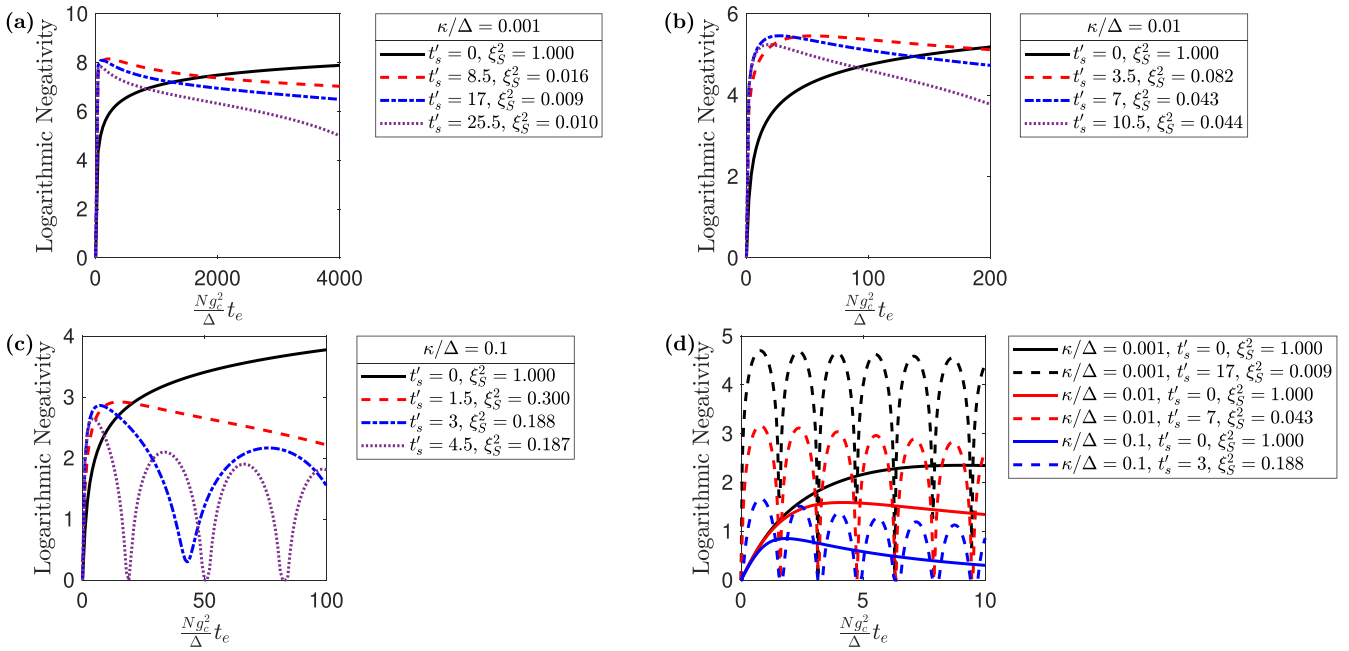

FIG. 8. Time evolution of logarithmic negativity E_N against dimensionless entanglement time $(Ng_c^2/\Delta)t_e$ in the photon-photon scenario for the entanglement Hamiltonian (a) $H_{\text{ent},-}$ with $\kappa/\Delta = 0.001$, (b) $H_{\text{ent},-}$ with $\kappa/\Delta = 0.01$, (c) $H_{\text{ent},-}$ with $\kappa/\Delta = 0.1$, and (d) $H_{\text{ent},+}$ with $\kappa/\Delta = 0.001$, 0.01, and 0.1.

A range of photon decoherence factors $\kappa/\Delta = 0.001$, 0.01, and 0.1 are used in the calculation. Figure 8 show the time evolution of E_N for both $H_{\text{ent},-}$ [Figs. 8(a)–8(c)] and $H_{\text{ent},+}$ [Fig. 8(d)]. The time evolution for the case of no decoherence ($\kappa/\Delta = 0$) is not shown since in the limit of large N with no decoherence there is no limit for the magnitude of spin squeezing and E_N, so they can be made arbitrarily large.

For the entanglement Hamiltonian $H_{\text{ent},-}$, consistent with previous results, E_N is improved only initially, although this initial improvement now occupies a longer period of dimensionless entanglement time t'_e. Figures 8(a) and 8(b) indicate that with sufficiently small decoherence and large N, initial squeezing may help to enhance entanglement for a comparably longer t'_e. Figures 8(b) and 8(c) make it clear that after this initial period of improvement, eventually E_N with initial squeezing ceases to be better than that with no initial squeezing. In Fig. 8(a) this is not apparent since it occurs at a much later time. Interestingly, Fig. 8(c) also reveals some pattern of periodicity in the time evolution of E_N with initial squeezing.

So far for $H_{\text{ent},-}$, we have observed the same general pattern in all scenarios, regardless of whether N is small or very large, that the presence of decoherence will cause E_N with initial squeezing to eventually cease to be better than that with no initial squeezing. While the approach for small N is not particularly illuminating with respect to this, the analysis for the large-N limit reveals additional insights into how decoherence affects the general patterns observed in all the results (including those of the phonon-photon and phonon-phonon scenarios). The reason for this pattern can be inferred from the effect of decoherence on the rotation of the spins. The spins are initially aligned with polar angle $\theta = \pi/2$. As initial squeezing is applied, the angle θ increases due to decoherence according to the rotation rate $\dot{\theta}$ given in Eq. (40). So by the end of initial squeezing, θ will be greater than $\pi/2$. Under the entanglement Hamiltonian $H_{\text{ent},-}$, the time evolution of the Wigner characteristic function corresponding to the decoherence contains terms that become greater overall in magnitude as θ becomes greater than $\pi/2$ (see Appendix D). In other words, with a greater initial increment of angle θ due to initial squeezing, decoherence has a greater impact on E_N relative to the situation of no squeezing. In addition, under this entanglement Hamiltonian, there is no further rotation ($\dot{\theta} = 0$) and the angle θ is a constant. Therefore, the spins with no initial squeezing experience less impact from decoherence at all times compared to the situation with initial squeezing since its angle remains constant at $\theta = \pi/2$. So although initial squeezing improves E_N initially against a greater effect of decoherence, eventually the effect of decoherence takes over and nullifies this improvement.

The time evolution of E_N in the case of the entanglement Hamiltonian $H_{\text{ent},+}$ is shown in Fig. 8(d). It is shown that initial squeezing improves E_N with appropriate squeezing time, consistent with previous results. A prominent pattern of periodicity also appears in this case. This pattern of periodicity is also noticeable in previous results for small N, although it is less pronounced.

Now we comment on this pattern of periodicity or oscillatory behavior in the entanglement. First, it is reasonable to assume that the decoherence considered here can only have a deleterious effect on the entanglement, i.e., it reduces the overall entanglement over time. Therefore, it should not contribute to the observed oscillatory behavior. Taking this into consideration, we then compute the time evolution of covariance matrix elements without decoherence for some fixed angle θ which is given in Appendix D. The result clearly shows oscillatory behavior which is caused by the existence of sinusoidal terms in the solution with a period of $\pi\Delta/2Ng_c^2$ for $H_{\text{ent},+}$. These sinusoidal terms happen to cancel

each other out if the initial state is the coherent spin state. This is the reason why under no initial squeezing there is no oscillation in entanglement, while oscillatory behavior is observed when initial squeezing is applied. In fact, there are also sinusoidal terms in the solution for $H_{\text{ent},-}$, with a period of $\pi\Delta/2Ng_c^2\cos^2\theta$. In this case, the longer initial squeezing is applied, the shorter the period of oscillation is, as can be seen in Fig. 8(c), because the angle θ becomes increasingly greater than $\pi/2$ the longer initial squeezing is applied. These terms also cancel each other out if the initial state is the coherent spin state. In summary, periodicity and oscillatory behavior are inherent natural features of both $H_{\text{ent},+}$ and $H_{\text{ent},-}$. Only in a special case, such as when the coherent spin state is the initial state (i.e., no initial squeezing), the oscillatory behavior disappears. Such oscillatory behavior is not uncommon and it has been exhibited, for example, in the Hamiltonians studied in Ref. [33].

For the entanglement Hamiltonian $H_{\text{ent},+}$, decoherence causes a nonzero rotation rate of the polar angle θ (see Appendix D). As θ gets larger, so does the effect of entanglement, because the time evolution of the Wigner characteristic function corresponding to the decoherence contains terms that become greater overall in magnitude as θ becomes greater than $\pi/2$. This is regardless of whether initial squeezing is applied or not; both experience an increasing effect of decoherence due to increasing θ. Under this condition, the results show that initial squeezing can provide enhancement of entanglement overall, even with some initial increment of angle $\theta > \pi/2$ due to initial squeezing. The presence of rotation is also the reason why E_N for $H_{\text{ent},+}$ is lower compared to that of $H_{\text{ent},-}$ over time, due to the increasing effect of decoherence.

It is appropriate to comment on the rotation rates $\dot{\theta}$ in $H_{\text{ent},+}$ and $H_{\text{ent},-}$ with respect to dissipative decoherence. Without decoherence, it is shown that $\dot{\theta} = 0$ for both $H_{\text{ent},+}$ and $H_{\text{ent},-}$, indicating that energy is conserved. With decoherence, energy dissipation should drive the spin states towards the minimum energy state, i.e., $\theta = \pi$. This can be observed for $H_{\text{ent},+}$ with $\dot{\theta} = \kappa N g_c^2 \sin\theta/\Delta^2$. However, for $H_{\text{ent},-}$, it is zero. In the analysis in the large-N limit, we have ignored terms with a coefficient much less than N in the time evolution of the Wigner characteristic function. Some of these terms for the decoherence in fact cause rotation, but when N is taken to be very large, i.e., $N \to \infty$, this rotation rate vanishes. When N is small however, this rotation rate should appear. Figure 9 shows the time evolution of the polar angle θ under decoherence for the phonon-phonon scenario with $N = 50$. It is shown that there is indeed a nonzero $\dot{\theta}$ for $H_{\text{ent},-}$ and, by extension, there exists energy dissipation in the system. This indicates that for $H_{\text{ent},-}$, the rate at which decoherence takes energy away from the system does not scale comparably with N. At the extreme limit of very large N, although energy dissipation still occurs, it is not enough to change the polar angle θ appreciably within the relevant timescale. Therefore, $\dot{\theta}$ appears to vanish in this limit. Even with small $N = 50$, $\dot{\theta}$ for $H_{\text{ent},-}$ is considerably smaller than that for $H_{\text{ent},+}$, especially with no initial squeezing. This renders the previous discussion in the large-N limit regarding the effects of decoherence and rotation still applicable also for small N. In addition, these facts also explain why in the results shown $H_{\text{ent},-}$ is more robust against dissipative decoherence compared to $H_{\text{ent},+}$.

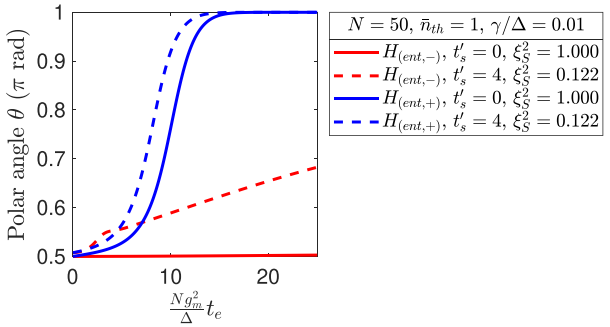

FIG. 9. Time evolution of θ under decoherence in the phonon-phonon scenario with no initial squeezing $t_s' = 0$ (solid lines) and with initial squeezing $t_s' = 4$ (dashed lines) for both $H_{\text{ent},-}$ (red) and $H_{\text{ent},+}$ (blue). The parameters are $N = 50$, $\bar{n}_{th} = 1$, and $\gamma/\Delta = 0.01$. With initial squeezing, the starting angle $\theta > \pi/2$.

The inclusion of the large number of spins allows for a more relaxed assumption of experimental parameters. Assuming that $\omega_c/2\pi \sim 1$ GHz and $Q = 10^3$, we get $\kappa/2\pi \sim 1$ MHz. This corresponds to $\Delta/2\pi = 100$ MHz for $\kappa/\Delta = 0.01$. With a coupling strength of $g_c/2\pi \sim 10$ Hz, for $N = 10^{12}$, the dimensionless entanglement time of $t_e' = 4000$ corresponds to $t_e \approx 6 \times 10^{-4}$ s. So, although the individual coupling strength of the NV center to the cavity resonator is small, the inclusion of the large number of spins compensates for this and allows for a much faster response time.

Finally, as mentioned at the beginning of Sec. II, the coupling strength of individual spins may be nonuniform, which causes a reduction of the effective number of spins. The results presented here are based on the effective number of spins. For example, if the effective number of spins is reduced by a factor of 2, this means that results for $N = 50$ in the phonon-photon (Sec. IV A) and phonon-phonon (Sec. IV B) scenarios correspond to an actual spin number of 100 in each ensemble. In the photon-photon scenario (Sec. IV A), a choice of $N = 10^{12}$ corresponds to an actual spin number of 2×10^{12} for a reduction factor of 2, which is still of the same order of magnitude. Of course, if there is little to no reduction due to approximately uniform coupling, then N may refer to both the effective and the actual number of spins.

V. CONCLUSION

In summary, we have investigated the effect of initial squeezing, governed by the one-axis twisting Hamiltonian, to entanglement of two NV-center ensembles under the influence of dissipative decoherence. To this end, we considered different possible means by which initial squeezing and entanglement are applied, namely, the phonon-photon, phonon-phonon, and photon-photon scenarios. In the entanglement timescale estimation of the phonon-photon scenario, the relevant timescale for entanglement dynamics is not fast enough relative to coherence times T_1 and T_2. This is the limitation in this scenario and it forms the motivation to consider the phonon-phonon scenario, in which coupling strength is increased, and the photon-photon scenario, in which the number of spins is increased. While the phonon-photon and phonon-phonon scenarios involve a relatively small number of

spins ($N \leqslant 100$), in the photon-photon scenario we consider the limit of a very large number of spins. The theoretical model for the entanglement is based on the Tavis-Cummings model, in which we take into account two possibilities of the opposite [$H_{\text{ent},-}$, Eq. (9)] and the same [$H_{\text{ent},+}$, Eq. (13)] signs of the coupling terms for the two ensembles in the coupling terms of the Hamiltonian.

In general, the results show that for the entanglement Hamiltonian $H_{\text{ent},-}$ initial squeezing improves logarithmic negativity E_N only initially, while for $H_{\text{ent},+}$ it improves E_N overall with an appropriate initial squeezing time. There are two important pieces of insight that contribute to this pattern. First, without decoherence, for $H_{\text{ent},-}$ initial squeezing improves E_N at the beginning, but it does not increase further at later time as compared to the case of no initial squeezing. We found that this is because there is an upper bound to entanglement at which saturation occurs. Without initial squeezing, E_N already saturates close to this bound for $H_{\text{ent},-}$ so that initial squeezing cannot increase E_N further. In contrast, for $H_{\text{ent},+}$ without initial squeezing, E_N does not saturate near this bound. Therefore, performing initial squeezing increases E_N further, up to this bound at saturation.

The second important observation is that the presence of decoherence causes the curves for E_N to slope downward eventually with time, but its behavior is different between $H_{\text{ent},-}$ and $H_{\text{ent},+}$. For $H_{\text{ent},-}$, it causes E_N with initial squeezing to eventually be lower than that without initial squeezing at later time. However, for $H_{\text{ent},+}$, E_N with initial squeezing is consistently higher at later time compared to that without initial squeezing. The reason for this difference is revealed in our analysis of the time evolution of the Wigner characteristic function in the limit of a very large number of spins, which incorporates the dynamics of rotation. The dissipative decoherence does not induce polar angle rotation of the mean spin direction for $H_{\text{ent},-}$, while it does for initial squeezing by H_{sq}. Therefore, the application of initial squeezing makes the initial angle larger. So even if initial squeezing increases E_N initially, this improvement is eventually taken over by the greater effect of decoherence due to the larger angle. The situation is different for $H_{\text{ent},+}$, as dissipative decoherence does induce polar angle rotation of the mean spin direction in this case. In the presence of rotation causing an increasing effect of decoherence whether or not initial squeezing is applied, an application of optimal initial squeezing can provide an improvement to logarithmic negativity overall relative to no initial squeezing.

As mentioned above, in the analysis in the large-N limit under dissipative decoherence, the polar angle rotation rate $\dot{\theta}$ is zero for $H_{\text{ent},-}$, while it is positive for $H_{\text{ent},+}$. This is because for $H_{\text{ent},-}$, the rate at which decoherence takes energy away from the system does not scale proportionally to N. It is shown that even for a relatively small $N = 50$, $\dot{\theta}$ is considerably smaller for $H_{\text{ent},-}$ than that for $H_{\text{ent},+}$. In the extreme case of the large-N limit, i.e., $N \to \infty$, $\dot{\theta}$ vanishes. Therefore, even if energy still dissipates from the system, the rate is not enough to change the polar angle θ appreciably within the relevant timescale. This explains why the results show that $H_{\text{ent},-}$ is more robust than $H_{\text{ent},+}$ against dissipation.

Finally, as the model used in this article is realistic and quite general, it should also be applicable to other systems. For example, the neutral divacancy defect in the cubic silicon carbide also has a spin-1 triplet ground state similar to the negatively charged NV center [67]. Other than solid-state systems, the model and results here should also be applicable to other systems, like cold atoms and trapped ions, for example, as long as they are described by the same Hamiltonians.

ACKNOWLEDGMENTS

We thank Abdullah Rasmita, Weibo Gao, and Shau-Yu Lan from the Division of Physics and Applied Physics, Nanyang Technological University, for helpful discussion. We are also grateful to the referees for their constructive feedback.

APPENDIX A: DICKE STATE BASIS

Consider two particles with spin quantum numbers s_1 and s_2. We can write down the collective spin vector operator as

$$\mathbf{J} = \mathbf{J}_1 + \mathbf{J}_2 \tag{A1}$$

and define basis state $|s, m_s\rangle$ such that

$$\mathbf{J}^2|s, m_s\rangle = s(s+1)|s, m_s\rangle, \tag{A2}$$

$$J_z|s, m_s\rangle = m_s|s, m_s\rangle, \tag{A3}$$

where $s = |s_1 - s_2|, |s_1 - s_2| + 1, \ldots, s_1 + s_2 - 1, s_1 + s_2$ and $m_s = -s, -s+1, \ldots, s-1, s$. As an example, for two qubits ($s_1 = s_2 = \frac{1}{2}$), using the properties given in Eqs. (A2) and (A3), it can be checked that $|s = 0, m_s = 0\rangle = \frac{1}{\sqrt{2}}(|\downarrow\uparrow\rangle - |\uparrow\downarrow\rangle)$, $|s = 1, m_s = -1\rangle = |\downarrow\downarrow\rangle$, $|s = 1, m_s = 0\rangle = \frac{1}{\sqrt{2}}(|\downarrow\uparrow\rangle + |\uparrow\downarrow\rangle)$, and $|s = 1, m_s = 1\rangle = |\uparrow\uparrow\rangle$, where we have used $|\uparrow\rangle$ and $|\downarrow\rangle$ to denote spin-up and spin-down, respectively.

The Dicke state $|D_k^N\rangle$ is defined as a superposition of all combinations of N qubits with the same number of spin-up k with uniform probability amplitudes. For example, $|D_2^3\rangle = \frac{1}{\sqrt{3}}(|\uparrow\uparrow\downarrow\rangle + |\uparrow\downarrow\uparrow\rangle + |\downarrow\uparrow\uparrow\rangle)$. In the case of $N = 2$ qubits, $|D_0^2\rangle = |\downarrow\downarrow\rangle \equiv |s = 1, m_s = -1\rangle$, $|D_1^2\rangle = \frac{1}{\sqrt{2}}(|\downarrow\uparrow\rangle + |\uparrow\downarrow\rangle) \equiv |s = 1, m_s = 0\rangle$, and $|D_2^2\rangle = |\uparrow\uparrow\rangle \equiv |s = 1, m_s = 1\rangle$. So, in this two-particle example, the Dicke states are states $|s, m_s\rangle$ with the highest $s = s_1 + s_2$.

The same can likewise be done for a general number N of particles with spin $\frac{1}{2}$, with collective spin operators $J_z = 1/2\sum_{i=1}^N \sigma_i^z$ and $J_\pm = \sum_{i=1}^N \sigma_i^\pm$. Indeed, it can be verified for any N and k that $\mathbf{J}^2|D_k^N\rangle = \frac{N}{2}(\frac{N}{2}+1)|D_k^N\rangle$ and $J_z|D_k^N\rangle = (k - \frac{N}{2})|D_k^N\rangle$, with $s = \frac{N}{2}$ and $m_s = k - \frac{N}{2}$. Thus, the Dicke states are simply states with the highest $s = \frac{N}{2}$, i.e., $|\frac{N}{2}, m_s\rangle$. For simplicity of notation, $|m\rangle$ will be used to denote $|\frac{N}{2}, m_s\rangle$, with $m = -\frac{N}{2}, -\frac{N}{2}+1, \ldots, \frac{N}{2}-1, \frac{N}{2}$, and this will serve as the Dicke state basis.

Let us discuss the initial coherent spin state $|\psi\rangle = [\frac{1}{\sqrt{2}}(|-1\rangle + |+1\rangle)]^{\otimes N}$ in the main text. Because here the individual spin is a two-level system, the two-level $|-1\rangle$ and $|+1\rangle$ states are equivalent to two-level $|\downarrow\rangle$ and $|\uparrow\rangle$ states. Measurement of the spin in the z axis direction has possible outcomes $-\frac{N}{2}, \ldots, \frac{N}{2}$ with binomial probability distribution.

Therefore, $|\psi\rangle$ expressed in the Dicke basis is

$$|\psi_D\rangle = \sum_{n=0}^{N} \left[\frac{N!}{2^N n!(N-n)!}\right]^{1/2} \left|n - \frac{N}{2}\right\rangle. \tag{A4}$$

In this basis, the collective spin operators can be written as square matrices of dimension $N+1$ that satisfy

$$\langle m'|\mathbf{J}^2|m\rangle = \delta_{m',m}\frac{N}{2}\left(\frac{N}{2}+1\right), \tag{A5a}$$

$$\langle m'|J_z|m\rangle = \delta_{m',m}m, \tag{A5b}$$

$$\langle m'|J_x|m\rangle = \frac{1}{2}(\delta_{m',m+1} + \delta_{m'+1,m}) \times\sqrt{\frac{N}{2}\left(\frac{N}{2}+1\right) - m'm}, \tag{A5c}$$

$$\langle m'|J_y|m\rangle = \frac{1}{2i}(\delta_{m',m+1} - \delta_{m'+1,m}) \times\sqrt{\frac{N}{2}\left(\frac{N}{2}+1\right) - m'm}, \tag{A5d}$$

$$\langle m'|J_+|m\rangle = \delta_{m',m+1}\sqrt{\frac{N}{2}\left(\frac{N}{2}+1\right) - m'm}, \tag{A5e}$$

$$\langle m'|J_-|m\rangle = \delta_{m'+1,m}\sqrt{\frac{N}{2}\left(\frac{N}{2}+1\right) - m'm}. \tag{A5f}$$

APPENDIX B: DYNAMICAL DECOUPLING ANALYSIS FOR $N = 6$

Here we consider dynamical decoupling applied to an isotopically pure NV sample (0.01% ^{13}C) as in Ref. [3]. In this system, the dominant interaction is with electronic spins of the surrounding nitrogen impurities (electron paramagnetic resonance spectrum centers), forming an electronic spin bath. The interaction between an NV-center spin and the random magnetic field from this spin bath can be written as

$$H_b = \tfrac{1}{2}b(t)\sigma_z, \tag{B1}$$

where $b(t) = g_e\mu_B B_{z,\mathrm{bath}}(t)/\hbar$ and $\sigma_z/2$ is the z axis single-spin operator. The random fluctuation in $b(t)$, resulting from the random magnetic field $B_{z,\mathrm{bath}}(t)$ created by the spin bath, can be modeled by an Ornstein-Uhlenbeck (OU) process [49,68–70], with the correlation function $\langle b(0)b(t)\rangle = L_b^2\exp(-R|t|)$, where L_b is the coupling strength of the bath to the NV spin and $1/R$ is the bath correlation time. The free decay of the coherence induced by the spin bath follows the Gaussian function $\exp(-L_b^2t^2/2)$ [49], which yields an estimated value $L_b \sim 2$ ms^{-1} obtained from Ref. [3].

Dynamical decoupling is applied using an n-pulse Carr-Purcell-Meiboom-Gill (CPMG) sequence, which results in a coherence time of $T_2 = (12n^2/L_b^2R)^{1/3}$ [49]. A coherence time of $T_2 \approx 580$ ms is obtained for $n \approx 8200$ pulses at 77 K [3], which gives an estimate of $R \sim 1$ ms^{-1}.

The estimated parameters obtained allow for simulation of the time evolution with Eq. (B1) under the OU process. More precisely, the free decay of the transverse component of a single NV spin [70]

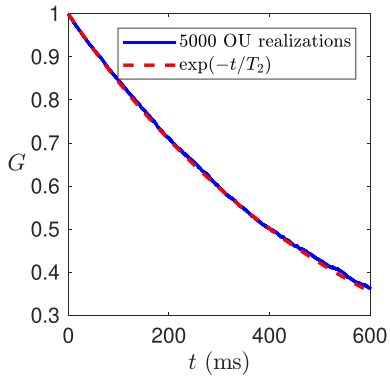

FIG. 10. Free decay of the transverse component of a single NV spin $G(t)$ as a function of time in the spin bath with an 8200-pulse CPMG decoupling sequence for 5000 OU realizations (blue solid line), fitted against the exponential decay function $\exp(-t/T_2)$ (red dashed line), with $T_2 = 580$ ms.

$$G(t) = \left\langle \exp\left(-i\int_0^t b(s)ds\right)\right\rangle \tag{B2}$$

is simulated, where the average is taken over the realizations of $b(s)$. The CPMG decoupling sequence is applied along the x axis.

The simulation result for 5000 realizations of OU processes with the CPMG decoupling sequence is shown in Fig. 10. The OU result is fitted against the exponential decay function $\exp(-t/T_2)$ and very good agreement is obtained. The fact that it fits very well with the exponential decay function suggests that the time evolution of an ensemble of N NV-center spins under dephasing due to the spin bath, combined with the CPMG decoupling sequence, can be represented by an effective Markovian master equation

$$\dot{\rho}_{T_2} = \frac{1}{2T_2}\sum_i^N \left(\sigma_i^z\rho\sigma_i^z - \rho\right). \tag{B3}$$

In other words, simulation of many realizations using Eq. (B1) under the OU process with the CPMG sequence can be replaced with a single time evolution using the master equation (B3).

Although the analysis of the bath-induced decoherence has been considerably simplified with the Markovian master equation, this still presents a challenge because it involves an individual spin operator instead of a collective one. Physically, this means that the bath-induced decoherence affects individual NV spins separately and as a result the spins in an ensemble cannot be treated as a single collective state. Therefore, the Dicke state basis approach presented in Appendix A, which treats an ensemble as a single collective state, cannot be implemented anymore. As a consequence, the full Hilbert space of dimension 2^N for a single ensemble (2^{2N} for two ensembles) must be taken into account. The time evolution of the spin state in this full Hilbert space is necessary in order to obtain the full information required to quantify the entanglement. Since the full Hilbert space dimension grows exponentially with N, numerical computation becomes impractical even for a relatively small N of 50–100. Therefore,

under this condition, here we consider a manageable number of $N = 6$ spins. Aside from that, in the limit of large N, the assumption of Gaussian states would not apply anymore. However, this is somewhat less of an issue since the important timescale for entanglement in the large-N limit can be much shorter or faster than T_2.

Figures 5(a) and 6(a) show that the patterns of entanglement for $N = 50$ and $N = 100$ are similar in the scaled dimensionless entanglement timescale $t'_e = (Ng_m^2/\Delta)t_e$. In the real timescale, however, a smaller N will occupy a longer period of time since $t_e \propto 1/N$ for some fixed value of scaled time t'_e. For $N = 6$, the entanglement timescale may considerably exceed T_2 so that no significant entanglement occurs. Therefore, here we modify the parameter g_m^2/Δ for $N = 6$ so that it captures the important entanglement dynamics at a real timescale comparable to that of $N \sim 50$–100. More specifically, we are looking into the entanglement dynamics up to $t_e = 100$ ms. Under this consideration, the parameter chosen for $N = 6$ is $g_m^2/2\pi\Delta = 7$ Hz. We emphasize that although we have modified the parameter, it is not the actual entanglement dynamics of $N = 6$ that is of concern, but rather how decoherence with associated coherence time T_2 affects the important entanglement dynamics within the specified timescale up to $t_e = 100$ ms, which corresponds more to a timescale of $N \sim 50$–100.

To test the validity of the Markovian dephasing in Eq. (B3) in our entanglement scenario, we first simulate the time evolution using (B3) together with the initial squeezing Hamiltonian H_{sq} [Eq. (4)] and subsequent entanglement Hamiltonians $H_{\text{ent},-}$ [Eq. (9)] and $H_{\text{ent},+}$ [Eq. (13)] without dissipative decoherence for the phonon-phonon scenario. Then we compare the results to those obtained by averaging 5000 realizations of OU processes using the Hamiltonian (B1). In both situations, the CPMG decoupling sequence is applied along the x axis. The reason why we ignore dissipative decoherence first is so that the computation of a single realization of the OU process only involves the time evolution of a pure state instead of mixed state; the computational simulation for a mixed state with the OU process would be impractical in particular since it needs to be repeated for thousands of realizations. The results for logarithmic negativity are presented in Fig. 11, showing a perfect match between the OU process and the Markovian master-equation approach. Thus, this validates the use of Markovian dephasing in Eq. (B3). Note that we do not consider the phonon-photon scenario here because we concluded in the main text that the entanglement timescale would be much larger than T_2 and so it would not be helpful to consider this scenario.

Now we are able to simulate the full dynamics of the system under initial squeezing and subsequent entanglement together with dissipative decoherence and the Markovian dephasing, applying the CPMG decoupling sequence along the x axis. Then we compare the results to the dynamics without Markovian dephasing and dynamical decoupling, as in the main text. The results are shown in Fig. 12. They show that the initial rise and the peaks of entanglement after this rise are relatively close to each other in value. Therefore, as long as the entanglement timescale involved is less than that of T_2, ignoring the effect of decoherence associated with coherence time T_2 is still a good approximation. More

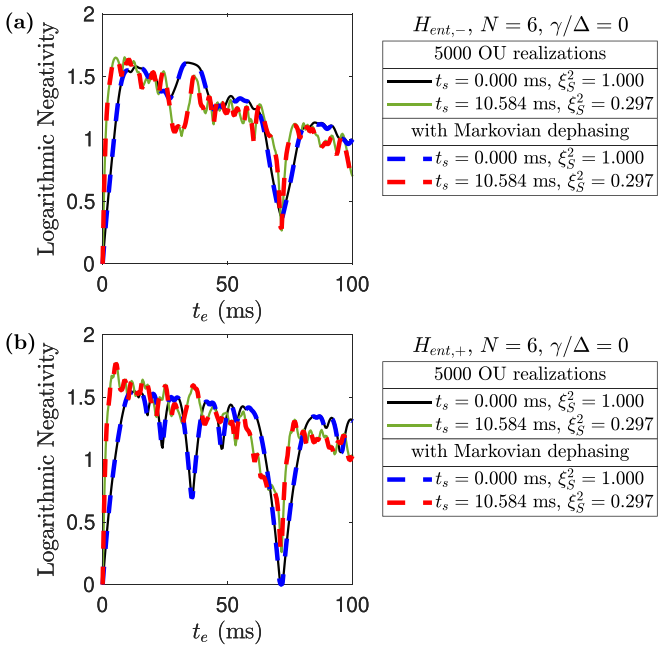

FIG. 11. Time evolution of logarithmic negativity E_N against entanglement time t_e in the phonon-phonon scenario with $N = 6$ and no dissipative decoherence $\gamma/\Delta = 0$ for the entanglement Hamiltonian (a) $H_{\text{ent},-}$ and (b) $H_{\text{ent},+}$. Here we consider a simulation with 5000 OU realizations (solid lines) and with Markovian dephasing (dashed lines).

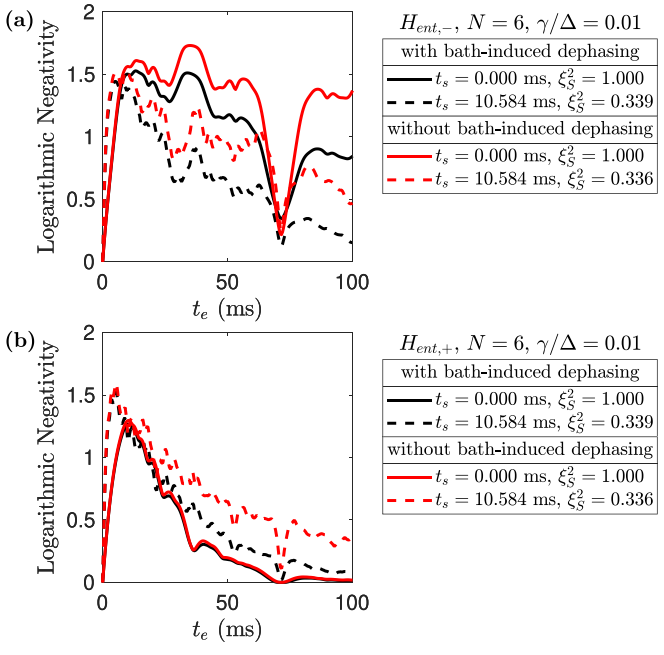

FIG. 12. Time evolution of logarithmic negativity E_N against entanglement time t_e in the phonon-phonon scenario with $N = 6$ and $\gamma/\Delta = 0.01$ for the entanglement Hamiltonian (a) $H_{\text{ent},-}$ and (b) $H_{\text{ent},+}$. Results for time evolution with spin-bath-induced dephasing (black solid lines and black dashed lines) are obtained using the Markovian dephasing master equation.

importantly, while the two results may show some differences quantitatively, it still retains the important qualitative features of entanglement enhancement, namely, that initial squeezing may enhance overall entanglement for the entanglement Hamiltonian $H_{\text{ent},+}$, while it enhances entanglement only initially for $H_{\text{ent},-}$.

Finally, although we consider an isotopically pure sample, the authors in Ref. [3] comment that similar results for coherence time T_2 can also be obtained for a naturally abundant sample (1.1% ^{13}C). Moreover, $T_2 \approx 0.6$ s is not an experimental limit as it can be further improved by using more optimal pulses and decoupling sequences. Furthermore, if the temperature considered is in the tens of millikelvin range, T_2 should be even longer.

APPENDIX C: OPERATOR CORRESPONDENCE

By applying the Baker-Campbell-Hausdorff (BCH) formula, the Wigner characteristic function $W(u,v) = \text{Tr}[\rho \exp(u\hat{x} + v\hat{p})]$ can be alternatively written as

$$W(u,v) = \text{Tr}[\rho \exp(u\hat{x}) \exp(v\hat{p})] \exp\left(-i\frac{uv}{2}\right) \quad \text{(C1a)}$$

$$= \text{Tr}[\rho \exp(v\hat{p}) \exp(u\hat{x})] \exp\left(i\frac{uv}{2}\right). \quad \text{(C1b)}$$

Differentiating these alternative forms with respect to u and v gives

$$\frac{\partial}{\partial u} W(u,v) = \text{Tr}[\rho\hat{x} \exp(u\hat{x}) \exp(v\hat{p})] \exp\left(-i\frac{uv}{2}\right) - i\frac{v}{2} W(u,v) \quad \text{(C2a)}$$

$$= \text{Tr}[\hat{x}\rho \exp(v\hat{p}) \exp(u\hat{x})] \exp\left(i\frac{uv}{2}\right) + i\frac{v}{2} W(u,v), \quad \text{(C2b)}$$

$$\frac{\partial}{\partial v} W(u,v) = \text{Tr}[\hat{p}\rho \exp(u\hat{x}) \exp(v\hat{p})] \exp\left(-i\frac{uv}{2}\right) - i\frac{u}{2} W(u,v) \quad \text{(C2c)}$$

$$= \text{Tr}[\rho\hat{p} \exp(v\hat{p}) \exp(u\hat{x})] \exp\left(i\frac{uv}{2}\right) + i\frac{u}{2} W(u,v). \quad \text{(C2d)}$$

Therefore, similar to how $W(u,v) = \text{Tr}[\rho \exp(u\hat{x} + v\hat{p})]$ corresponds to the state ρ, by rearranging we obtain the correspondence

$$\rho\hat{x} \to \text{Tr}[\rho\hat{x} \exp(u\hat{x} + v\hat{p})] = \left(\frac{\partial}{\partial u} + i\frac{v}{2}\right) W(u,v), \quad \text{(C3a)}$$

$$\hat{x}\rho \to \text{Tr}[\hat{x}\rho \exp(u\hat{x} + v\hat{p})] = \left(\frac{\partial}{\partial u} - i\frac{v}{2}\right) W(u,v), \quad \text{(C3b)}$$

$$\hat{p}\rho \to \text{Tr}[\hat{p}\rho \exp(u\hat{x} + v\hat{p})] = \left(\frac{\partial}{\partial v} + i\frac{u}{2}\right) W(u,v), \quad \text{(C3c)}$$

$$\rho\hat{p} \to \text{Tr}[\rho\hat{p} \exp(u\hat{x} + v\hat{p})] = \left(\frac{\partial}{\partial v} - i\frac{u}{2}\right) W(u,v), \quad \text{(C3d)}$$

where the BCH formula has been applied. So the action of $\hat{x}$ or $\hat{p}$ on ρ has a corresponding differential operation on $W(u,v)$. This correspondence can be further extended to the action of the second-order quadrature operators on ρ. For example,

$$\rho\hat{x}\hat{p} \to \left(\frac{\partial}{\partial v} - i\frac{u}{2}\right)\left(\frac{\partial}{\partial u} + i\frac{v}{2}\right) W(u,v), \quad \text{(C4)}$$

$$\hat{x}\hat{p}\rho \to \left(\frac{\partial}{\partial u} - i\frac{v}{2}\right)\left(\frac{\partial}{\partial v} + i\frac{u}{2}\right) W(u,v), \quad \text{(C5)}$$

$$\hat{x}\rho\hat{p} \to \left(\frac{\partial}{\partial u} - i\frac{v}{2}\right)\left(\frac{\partial}{\partial v} - i\frac{u}{2}\right) W(u,v) = \left(\frac{\partial}{\partial v} - i\frac{u}{2}\right)\left(\frac{\partial}{\partial u} - i\frac{v}{2}\right) W(u,v). \quad \text{(C6)}$$

Its validity can be demonstrated by differentiating the appropriate correspondence relation once more. As an example, for $\rho\hat{x}\hat{p}$, we start by differentiating the correspondence of $\rho\hat{x}$ with respect to v as follows:

$$\frac{\partial}{\partial v} \text{Tr}[\rho\hat{x} \exp(u\hat{x} + v\hat{p})] = \frac{\partial}{\partial v}\left(\frac{\partial}{\partial u} + i\frac{v}{2}\right) W(u,v),$$

$$\frac{\partial}{\partial v}\left[\text{Tr}[\rho\hat{x} \exp(v\hat{p}) \exp(u\hat{x})] \exp\left(i\frac{uv}{2}\right)\right] = \frac{\partial}{\partial v}\left(\frac{\partial}{\partial u} + i\frac{v}{2}\right) W(u,v),$$

$$\text{Tr}[\rho\hat{x}\hat{p} \exp(v\hat{p}) \exp(u\hat{x})] \exp\left(i\frac{uv}{2}\right) + i\frac{u}{2}\left(\frac{\partial}{\partial u} + i\frac{v}{2}\right) W(u,v) = \frac{\partial}{\partial v}\left(\frac{\partial}{\partial u} + i\frac{v}{2}\right) W(u,v),$$

$$\text{Tr}[\rho\hat{x}\hat{p} \exp(u\hat{x} + v\hat{p})] = \left(\frac{\partial}{\partial v} - i\frac{u}{2}\right)\left(\frac{\partial}{\partial u} + i\frac{v}{2}\right) W(u,v). \quad \text{(C7)}$$

APPENDIX D: TIME EVOLUTION OF THE WIGNER CHARACTERISTIC FUNCTION AND COVARIANCE MATRIX

Here the time evolution of the Wigner characteristic function and covariance matrix elements for the entanglement Hamiltonians $H_{\text{ent},-}$ [Eq. (9)] and $H_{\text{ent},+}$ [Eq. (13)] and their respective decoherence (16) are given. As illustrated in the main text, the time evolution of the Wigner characteristic function is obtained by applying the coordinate transformation (28), Holstein-Primakoff

transformation, and operator correspondence (20) consecutively to the master equation, taking into account the rotating frame of reference.

First, for the master equation $\dot{\rho} = -i[H_{\text{ent},-}, \rho]$,

$$\dot{W}(\mathbf{V}, t_e) = \frac{Ng_c^2}{\Delta}\Bigg[\cos^2\theta(v_1+v_2)\left(\frac{\partial}{\partial u_1}+\frac{\partial}{\partial u_2}\right)+(1-2\cos^2\theta)\left(u_1\frac{\partial}{\partial v_1}+u_2\frac{\partial}{\partial v_2}\right)-u_1\frac{\partial}{\partial v_2}-u_2\frac{\partial}{\partial v_1}\Bigg]W(\mathbf{V}, t_e), \tag{D1}$$

where $\mathbf{V} = (u_1, v_1, u_2, v_2)^{\mathrm{T}}$. For its associated decoherence $\dot{\rho} = (g_c/\Delta)^2\kappa\mathcal{D}[F]\rho$ with $F = J_1^- - J_2^-$,

$$\dot{W}(\mathbf{V}, t_e) = \frac{Ng_c^2}{\Delta}\frac{\kappa}{2\Delta}\Bigg\{\frac{1}{2}(u_1-u_2)^2+\frac{1}{2}\cos^2\theta(v_1-v_2)^2+\cos\theta\Bigg[(u_1-u_2)\left(\frac{\partial}{\partial u_1}-\frac{\partial}{\partial u_2}\right)$$
$$+(v_1-v_2)\left(\frac{\partial}{\partial v_1}-\frac{\partial}{\partial v_2}\right)\Bigg]\Bigg\}W(\mathbf{V}, t_e). \tag{D2}$$

There is no rotation for $H_{\text{ent},-}$ and its associated decoherence, i.e., $\omega_z = 0$ and $\dot{\theta} = 0$. The time evolution for the covariance matrix elements is

$$\dot{\sigma}_{11} = \lambda\{2\sigma_{12}(1-2\cos^2\theta)-2\sigma_{14}+\epsilon[1+2(\sigma_{11}-\sigma_{13})\cos\theta]\}, \tag{D3a}$$
$$\dot{\sigma}_{22} = \lambda\{2(\sigma_{12}+\sigma_{23})\cos^2\theta+\epsilon[\cos^2\theta+2(\sigma_{22}-\sigma_{24})\cos\theta]\}, \tag{D3b}$$
$$\dot{\sigma}_{33} = \lambda\{2\sigma_{34}(1-2\cos^2\theta)-2\sigma_{23}+\epsilon[1+2(\sigma_{33}-\sigma_{13})\cos\theta]\}, \tag{D3c}$$
$$\dot{\sigma}_{44} = \lambda\{2(\sigma_{14}+\sigma_{34})\cos^2\theta+\epsilon[\cos^2\theta+2(\sigma_{44}-\sigma_{24})\cos\theta]\}, \tag{D3d}$$
$$\dot{\sigma}_{21} = \dot{\sigma}_{12} = \lambda\{(\sigma_{11}+\sigma_{13})\cos^2\theta+\sigma_{22}(1-2\cos^2\theta)-\sigma_{24}-\epsilon(\sigma_{14}+\sigma_{23}-2\sigma_{12})\cos\theta\}, \tag{D3e}$$
$$\dot{\sigma}_{31} = \dot{\sigma}_{13} = \lambda\{(\sigma_{14}+\sigma_{23})(1-2\cos^2\theta)-\sigma_{12}-\sigma_{34}-\epsilon[1+(\sigma_{11}+\sigma_{33}-2\sigma_{13})\cos\theta]\}, \tag{D3f}$$
$$\dot{\sigma}_{41} = \dot{\sigma}_{14} = \lambda\{(\sigma_{11}+\sigma_{13})\cos^2\theta+\sigma_{24}(1-2\cos^2\theta)-\sigma_{44}-\epsilon(\sigma_{12}+\sigma_{34}-2\sigma_{14})\cos\theta\}, \tag{D3g}$$
$$\dot{\sigma}_{32} = \dot{\sigma}_{23} = \lambda\{(\sigma_{13}+\sigma_{33})\cos^2\theta+\sigma_{24}(1-2\cos^2\theta)-\sigma_{22}-\epsilon(\sigma_{12}+\sigma_{34}-2\sigma_{23})\cos\theta\}, \tag{D3h}$$
$$\dot{\sigma}_{42} = \dot{\sigma}_{24} = \lambda\{(\sigma_{12}+\sigma_{14}+\sigma_{23}+\sigma_{34})\cos^2\theta-\epsilon[\cos^2\theta+(\sigma_{22}+\sigma_{44}-2\sigma_{24})\cos\theta]\}, \tag{D3i}$$
$$\dot{\sigma}_{43} = \dot{\sigma}_{34} = \lambda\{(\sigma_{13}+\sigma_{33})\cos^2\theta+\sigma_{44}(1-2\cos^2\theta)-\sigma_{24}-\epsilon(\sigma_{14}+\sigma_{23}-2\sigma_{34})\cos\theta\}, \tag{D3j}$$

where $\lambda = Ng_c^2/\Delta$, $\epsilon = \kappa/2\Delta$, and the fact that $\sigma_{21} = \sigma_{12}$, $\sigma_{31} = \sigma_{13}$, $\sigma_{41} = \sigma_{14}$, $\sigma_{32} = \sigma_{23}$, $\sigma_{42} = \sigma_{24}$, and $\sigma_{43} = \sigma_{34}$ has been used.

Furthermore, for identical ensembles, the covariance matrix is symmetrical under exchange. This introduces additional constraints of $\sigma_{33} = \sigma_{11}$, $\sigma_{44} = \sigma_{22}$, $\sigma_{34} = \sigma_{12}$, and $\sigma_{23} = \sigma_{14}$. If there is no decoherence, the reduced time evolution of elements of the covariance matrix for some fixed angle θ is given by

$$\dot{\sigma}_{11} = \lambda[2\sigma_{12}(1-2\cos^2\theta)-2\sigma_{14}], \tag{D4a}$$
$$\dot{\sigma}_{22} = \lambda[2(\sigma_{12}+\sigma_{14})\cos^2\theta], \tag{D4b}$$
$$\dot{\sigma}_{12} = \lambda[(\sigma_{11}+\sigma_{13})\cos^2\theta+\sigma_{22}(1-2\cos^2\theta)-\sigma_{24}], \tag{D4c}$$
$$\dot{\sigma}_{13} = \lambda[2\sigma_{14}(1-2\cos^2\theta)-2\sigma_{12}], \tag{D4d}$$
$$\dot{\sigma}_{14} = \lambda[(\sigma_{11}+\sigma_{13})\cos^2\theta+\sigma_{24}(1-2\cos^2\theta)-\sigma_{22}], \tag{D4e}$$
$$\dot{\sigma}_{24} = \lambda[2(\sigma_{12}+\sigma_{14})\cos^2\theta]. \tag{D4f}$$

In the following, let $c_\theta = \cos^2\theta$ and $k_\theta = \sin^2\theta = 1 - c_\theta$. For a fixed angle θ, the solution for the set of linear differential equations above can be written in the form $\mathbf{y}(t_e') = M^-\mathbf{y}(0)$, where $\mathbf{y} = (\sigma_{11}, \sigma_{22}, \sigma_{12}, \sigma_{13}, \sigma_{14}, \sigma_{24})^{\mathrm{T}}$, $t_e' = \lambda t_e$ is the dimensionless entanglement time, and $M^- = (M_L^-|M_R^-)$, with

$$M_L^- = \frac{1}{4}\begin{pmatrix} 3+\cos(4c_\theta t_e') & 1+8k_\theta^2 t_e'^2-\cos(4c_\theta t_e') & 8k_\theta t_e'-2\sin(4c_\theta t_e') \\ 1-\cos(4c_\theta t_e') & 3+\cos(4c_\theta t_e') & 2\sin(4c_\theta t_e') \\ \sin(4c_\theta t_e') & 4k_\theta t_e'-\sin(4c_\theta t_e') & 2+2\cos(4c_\theta t_e') \\ \cos(4c_\theta t_e')-1 & 1-8k_\theta^2 t_e'^2-\cos(4c_\theta t_e') & -8k_\theta t_e'-2\sin(4c_\theta t_e') \\ \sin(4c_\theta t_e') & -4k_\theta t_e'-\sin(4c_\theta t_e') & 2\cos(4c_\theta t_e')-2 \\ 1-\cos(4c_\theta t_e') & \cos(4c_\theta t_e')-1 & 2\sin(4c_\theta t_e') \end{pmatrix}, \tag{D5a}$$

$$M_R^- = \frac{1}{4}\begin{pmatrix} \cos(4c_\theta t_e') - 1 & -8k_\theta t_e' - 2\sin(4c_\theta t_e') & 1 - 8k_\theta^2 t_e'^2 - \cos(4c_\theta t_e') \\ 1 - \cos(4c_\theta t_e') & 2\sin(4c_\theta t_e') & \cos(4c_\theta t_e') - 1 \\ \sin(4c_\theta t_e') & 2\cos(4c_\theta t_e') - 2 & -4k_\theta t_e' - \sin(4c_\theta t_e') \\ 3 + \cos(4c_\theta t_e') & 8k_\theta t_e' - 2\sin(4c_\theta t_e') & 1 + 8k_\theta^2 t_e'^2 - \cos(4c_\theta t_e') \\ \sin(4c_\theta t_e') & 2 + 2\cos(4c_\theta t_e') & 4k_\theta t_e' - \sin(4c_\theta t_e') \\ 1 - \cos(4c_\theta t_e') & 2\sin(4c_\theta t_e') & 3 + \cos(4c_\theta t_e') \end{pmatrix}. \tag{D5b}$$

There are sinusoidal terms in the entries of M^-, all with a common period of $\pi/2\lambda\cos^2\theta$. For $\theta > \pi/2$, this causes oscillatory behavior in the solution for $\mathbf{y}$ and, by extension, the logarithmic negativity as well. Other than the condition that $\theta = \pi/2$, the oscillatory behavior can also disappear in some cases. For example, in a special case of initial state with $\sigma_{11} = \sigma_{22}$ and $\sigma_{12} = \sigma_{13} = \sigma_{14} = \sigma_{24} = 0$, the sinusoidal terms cancel each other in the solution. The coherent spin state is one such case.

Next, for the master equation $\dot\rho = -i[H_{\text{ent},+}, \rho]$,

$$\dot W(\mathbf{V}, t_e) = \frac{Ng_c^2}{\Delta}\left[(1+\sin^2\theta)\left(v_1\frac{\partial}{\partial u_1} + v_2\frac{\partial}{\partial u_2}\right) - \cos^2\theta\left(v_1\frac{\partial}{\partial u_2} + v_2\frac{\partial}{\partial u_1}\right) - (u_1 - u_2)\left(\frac{\partial}{\partial v_1} - \frac{\partial}{\partial v_2}\right)\right]W(\mathbf{V}, t_e). \tag{D6}$$

For its associated decoherence $\dot\rho = (g_c/\Delta)^2\kappa\mathcal{D}[F]\rho$ with $F = J_1^- + J_2^-$,

$$\dot W(\mathbf{V}, t_e) = \frac{Ng_c^2}{\Delta}\frac{\kappa}{2\Delta}\left\{\frac{1}{2}(u_1+u_2)^2 + \frac{1}{2}\cos^2\theta(v_1+v_2)^2 + \cos\theta\left[(u_1+u_2)\left(\frac{\partial}{\partial u_1} + \frac{\partial}{\partial u_2}\right) + (v_1+v_2)\left(\frac{\partial}{\partial v_1} + \frac{\partial}{\partial v_2}\right)\right]\right\}W(\mathbf{V}, t_e). \tag{D7}$$

The rotation rates corresponding to $H_{\text{ent},+}$ and its associated decoherence are

$$\omega_z = -2\frac{Ng_c^2}{\Delta}\cos\theta, \quad \dot\theta = \frac{\kappa N g_c^2}{\Delta^2}\sin\theta. \tag{D8}$$

The time evolution for the covariance matrix elements is

$$\dot\sigma_{11} = \lambda\{2(\sigma_{14} - \sigma_{12}) + \epsilon[1 + 2(\sigma_{11} + \sigma_{13})\cos\theta]\}, \tag{D9a}$$
$$\dot\sigma_{22} = \lambda\{2\sigma_{12}(1+\sin^2\theta) - 2\sigma_{23}\cos^2\theta + \epsilon[\cos^2\theta + 2(\sigma_{22} + \sigma_{24})\cos\theta]\}, \tag{D9b}$$
$$\dot\sigma_{33} = \lambda\{2(\sigma_{23} - \sigma_{34}) + \epsilon[1 + 2(\sigma_{13} + \sigma_{33})\cos\theta]\}, \tag{D9c}$$
$$\dot\sigma_{44} = \lambda\{2\sigma_{34}(1+\sin^2\theta) - 2\sigma_{14}\cos^2\theta + \epsilon[\cos^2\theta + 2(\sigma_{24} + \sigma_{44})\cos\theta]\}, \tag{D9d}$$
$$\dot\sigma_{21} = \dot\sigma_{12} = \lambda\{\sigma_{24} - \sigma_{22} + \sigma_{11}(1+\sin^2\theta) - \sigma_{13}\cos^2\theta + \epsilon(2\sigma_{12} + \sigma_{14} + \sigma_{23})\cos\theta\}, \tag{D9e}$$
$$\dot\sigma_{31} = \dot\sigma_{13} = \lambda\{\sigma_{12} + \sigma_{34} - \sigma_{14} - \sigma_{23} + \epsilon[1 + (\sigma_{11} + 2\sigma_{13} + \sigma_{33})\cos\theta]\}, \tag{D9f}$$
$$\dot\sigma_{41} = \dot\sigma_{14} = \lambda\{\sigma_{44} - \sigma_{24} + \sigma_{13}(1+\sin^2\theta) - \sigma_{11}\cos^2\theta + \epsilon(\sigma_{12} + 2\sigma_{14} + \sigma_{34})\cos\theta\}, \tag{D9g}$$
$$\dot\sigma_{32} = \dot\sigma_{23} = \lambda\{\sigma_{22} - \sigma_{24} + \sigma_{13}(1+\sin^2\theta) - \sigma_{33}\cos^2\theta + \epsilon(\sigma_{12} + 2\sigma_{23} + \sigma_{34})\cos\theta\}, \tag{D9h}$$
$$\dot\sigma_{42} = \dot\sigma_{24} = \lambda\{(\sigma_{14} + \sigma_{23})(1+\sin^2\theta) - (\sigma_{12} + \sigma_{34})\cos^2\theta + \epsilon[\cos^2\theta + (\sigma_{22} + 2\sigma_{24} + \sigma_{44})\cos\theta]\}, \tag{D9i}$$
$$\dot\sigma_{43} = \dot\sigma_{34} = \lambda\{\sigma_{24} - \sigma_{44} + \sigma_{33}(1+\sin^2\theta) - \sigma_{13}\cos^2\theta + \epsilon(\sigma_{14} + \sigma_{23} + 2\sigma_{34})\cos\theta\}, \tag{D9j}$$

where $\lambda = Ng_c^2/\Delta$, $\epsilon = \kappa/2\Delta$, and the fact that $\sigma_{21} = \sigma_{12}$, $\sigma_{31} = \sigma_{13}$, $\sigma_{41} = \sigma_{14}$, $\sigma_{32} = \sigma_{23}$, $\sigma_{42} = \sigma_{24}$, and $\sigma_{43} = \sigma_{34}$ has been used.

With the constraints $\sigma_{33} = \sigma_{11}$, $\sigma_{44} = \sigma_{22}$, $\sigma_{34} = \sigma_{12}$, and $\sigma_{23} = \sigma_{14}$ for identical ensembles and no decoherence for some fixed angle θ, the reduced time evolution is

$$\dot\sigma_{11} = \lambda[2(\sigma_{14} - \sigma_{12})], \tag{D10a}$$
$$\dot\sigma_{22} = \lambda[2\sigma_{12}(1+\sin^2\theta) - 2\sigma_{14}\cos^2\theta], \tag{D10b}$$
$$\dot\sigma_{12} = \lambda[\sigma_{24} - \sigma_{22} + \sigma_{11}(1+\sin^2\theta) - \sigma_{13}\cos^2\theta], \tag{D10c}$$
$$\dot\sigma_{13} = \lambda[2\sigma_{12} - 2\sigma_{14}], \tag{D10d}$$
$$\dot\sigma_{14} = \lambda[\sigma_{22} - \sigma_{24} + \sigma_{13}(1+\sin^2\theta) - \sigma_{11}\cos^2\theta], \tag{D10e}$$
$$\dot\sigma_{24} = \lambda[2\sigma_{14}(1+\sin^2\theta) - 2\sigma_{12}\cos^2\theta]. \tag{D10f}$$

In the following, let $c_\theta = \cos^2\theta$ and $k_\theta = \sin^2\theta = 1 - c_\theta$. For a fixed angle θ, the solution can be written in the form $\mathbf{y}(t_e') = M^+\mathbf{y}(0)$, where $\mathbf{y} = (\sigma_{11}, \sigma_{22}, \sigma_{12}, \sigma_{13}, \sigma_{14}, \sigma_{24})^{\mathrm{T}}$, $t_e' = \lambda t_e$ is the dimensionless entanglement time, and $M^+ = (M_L^+|M_R^+)$ with

$$M_L^+ = \frac{1}{4}\begin{pmatrix} 3+\cos(4t_e') & 1-\cos(4t_e') & -2\sin(4t_e') \\ 1+8k_\theta^2 t_e'^2-\cos(4t_e') & 3+\cos(4t_e') & 8k_\theta t_e'+2\sin(4t_e') \\ 4k_\theta t_e'+\sin(4t_e') & -\sin(4t_e') & 2+2\cos(4t_e') \\ 1-\cos(4t_e') & \cos(4t_e')-1 & 2\sin(4t_e') \\ 4k_\theta t_e'-\sin(4t_e') & \sin(4t_e') & 2-2\cos(4t_e') \\ 8k_\theta^2 t_e'^2+\cos(4t_e')-1 & 1-\cos(4t_e') & 8k_\theta t_e'-2\sin(4t_e') \end{pmatrix}, \tag{D11a}$$

$$M_R^+ = \frac{1}{4}\begin{pmatrix} 1-\cos(4t_e') & 2\sin(4t_e') & \cos(4t_e')-1 \\ 8k_\theta^2 t_e'^2+\cos(4t_e')-1 & 8k_\theta t_e'-2\sin(4t_e') & 1-\cos(4t_e') \\ 4k_\theta t_e'-\sin(4t_e') & 2-2\cos(4t_e') & \sin(4t_e') \\ 3+\cos(4t_e') & -2\sin(4t_e') & 1-\cos(4t_e') \\ 4k_\theta t_e'+\sin(4t_e') & 2+2\cos(4t_e') & -\sin(4t_e') \\ 1+8k_\theta^2 t_e'^2-\cos(4t_e') & 8k_\theta t_e'+2\sin(4t_e') & 3+\cos(4t_e') \end{pmatrix}. \tag{D11b}$$

There are sinusoidal terms in the entries of M^+, all with a common period of $\pi/2\lambda$. This in turn causes oscillatory behavior in the solution for $\mathbf{y}$ and, by extension, the logarithmic negativity as well. In some cases, oscillatory behavior may disappear. For example, in the special case of an initial state with $\sigma_{11} = \sigma_{22}$ and $\sigma_{12} = \sigma_{13} = \sigma_{14} = \sigma_{24} = 0$, the sinusoidal terms cancel each other in the solution. The coherent spin state is one such case.

[1] F. Jelezko and J. Wrachtrup, Single defect centres in diamond: A review, Phys. Status Solidi A **203**, 3207 (2006).

[2] G. Balasubramanian, P. Neumann, D. Twitchen, M. Markham, R. Kolesov, N. Mizuochi, J. Isoya, J. Achard, J. Beck, J. Tissler, V. Jacques, P. R. Hemmer, F. Jelezko, and J. Wrachtrup, Ultralong spin coherence time in isotopically engineered diamond, Nat. Mater. **8**, 383 (2009).

[3] N. Bar-Gill, L. M. Pham, A. Jarmola, D. Budker, and R. L. Walsworth, Solid-state electronic spin coherence time approaching one second, Nat. Commun. **4**, 1743 (2013).

[4] P. C. Maurer, G. Kucsko, C. Latta, L. Jiang, N. Y. Yao, S. D. Bennett, F. Pastawski, D. Hunger, N. Chisholm, M. Markham, D. J. Twitchen, J. I. Cirac, and M. D. Lukin, Room-temperature quantum bit memory exceeding one second, Science **336**, 1283 (2012).

[5] R. Hanson, F. M. Mendoza, R. J. Epstein, and D. D. Awschalom, Polarization and Readout of Coupled Single Spins in Diamond, Phys. Rev. Lett. **97**, 087601 (2006).

[6] G. D. Fuchs, V. V. Dobrovitski, R. Hanson, A. Batra, C. D. Weis, T. Schenkel, and D. D. Awschalom, Excited-State Spectroscopy using Single Spin Manipulation in Diamond, Phys. Rev. Lett. **101**, 117601 (2008).

[7] M. Hanks, M. Trupke, J. Schmiedmayer, W. J. Munro, and K. Nemoto, High-fidelity spin measurement on the nitrogen-vacancy center, New J. Phys. **19**, 103002 (2017).

[8] E. Togan, Y. Chu, A. S. Trifonov, L. Jiang, J. Maze, L. Childress, M. V. G. Dutt, A. S. Sørensen, P. R. Hemmer, A. S. Zibrov, and M. D. Lukin, Quantum entanglement between an optical photon and a solid-state spin qubit, Nature (London) **466**, 730 (2010).

[9] F. Dolde, I. Jakobi, B. Naydenov, N. Zhao, S. Pezzagna, C. Trautmann, J. Meijer, P. Neumann, F. Jelezko, and J. Wrachtrup, Room-temperature entanglement between single defect spins in diamond, Nat. Phys. **9**, 139 (2013).

[10] H. Bernien, B. Hensen, W. Pfaff, G. Koolstra, M. S. Blok, L. Robledo, T. H. Taminiau, M. Markham, D. J. Twitchen, L. Childress, and R. Hanson, Heralded entanglement between solid-state qubits separated by three metres, Nature (London) **497**, 86 (2013).

[11] T. Astner, S. Nevlacsil, N. Peterschofsky, A. Angerer, S. Rotter, S. Putz, J. Schmiedmayer, and J. Majer, Coherent Coupling of Remote Spin Ensembles via a Cavity Bus, Phys. Rev. Lett. **118**, 140502 (2017).

[12] S. D. Bennett, N. Y. Yao, J. Otterbach, P. Zoller, P. Rabl, and M. D. Lukin, Phonon-Induced Spin-Spin Interactions in Diamond Nanostructures: Application to Spin Squeezing, Phys. Rev. Lett. **110**, 156402 (2013).

[13] M. Kitagawa and M. Ueda, Squeezed spin states, Phys. Rev. A **47**, 5138 (1993).

[14] D. J. Wineland, J. J. Bollinger, W. M. Itano, F. L. Moore, and D. J. Heinzen, Spin squeezing and reduced quantum noise in spectroscopy, Phys. Rev. A **46**, R6797 (1992).

[15] D. J. Wineland, J. J. Bollinger, W. M. Itano, and D. J. Heinzen, Squeezed atomic states and projection noise in spectroscopy, Phys. Rev. A **50**, 67 (1994).

[16] E. S. Polzik, The squeeze goes on, Nature (London) **453**, 45 (2008).

[17] A. D. Cronin, J. Schmiedmayer, and D. E. Pritchard, Optics and interferometry with atoms and molecules, Rev. Mod. Phys. **81**, 1051 (2009).

[18] J. Ma, X. Wang, C. Sun, and F. Nori, Quantum spin squeezing, Phys. Rep. **509**, 89 (2011).

[19] A. Sørensen, L.-M. Duan, J. I. Cirac, and P. Zoller, Many-particle entanglement with Bose-Einstein condensates, Nature (London) **409**, 63 (2001).

[20] O. Gühne and G. Tóth, Entanglement detection, Phys. Rep. **474**, 1 (2009).

[21] B. Julsgaard, A. Kozhekin, and E. S. Polzik, Experimental long-lived entanglement of two macroscopic objects, Nature (London) **413**, 400 (2001).

[22] D. W. Berry and B. C. Sanders, Equivalence between two-mode spin squeezed states and pure entangled states with equal spin, J. Phys. A: Math. Gen. **38**, L205 (2005).

[23] M. G. Raymer, A. C. Funk, B. C. Sanders, and H. de Guise, Separability criterion for separate quantum systems, Phys. Rev. A **67**, 052104 (2003).

[24] A. S. Sørensen and K. Mølmer, Entanglement and Extreme Spin Squeezing, Phys. Rev. Lett. **86**, 4431 (2001).

[25] J. K. Korbicz, J. I. Cirac, and M. Lewenstein, Spin Squeezing Inequalities and Entanglement of n Qubit States, Phys. Rev. Lett. **95**, 120502 (2005).

[26] J. K. Korbicz, O. Gühne, M. Lewenstein, H. Häffner, C. F. Roos, and R. Blatt, Generalized spin-squeezing inequalities in n-qubit systems: Theory and experiment, Phys. Rev. A **74**, 052319 (2006).

[27] T. Fernholz, H. Krauter, K. Jensen, J. F. Sherson, A. S. Sørensen, and E. S. Polzik, Spin Squeezing of Atomic Ensembles via Nuclear-Electronic Spin Entanglement, Phys. Rev. Lett. **101**, 073601 (2008).

[28] A. Kuzmich, K. Mølmer, and E. S. Polzik, Spin Squeezing in an Ensemble of Atoms Illuminated with Squeezed Light, Phys. Rev. Lett. **79**, 4782 (1997).

[29] J. Hald, J. L. Sørensen, C. Schori, and E. S. Polzik, Spin Squeezed Atoms: A Macroscopic Entangled Ensemble Created by Light, Phys. Rev. Lett. **83**, 1319 (1999).

[30] K. Hammerer, E. S. Polzik, and J. I. Cirac, Teleportation and spin squeezing utilizing multimode entanglement of light with atoms, Phys. Rev. A **72**, 052313 (2005).

[31] R. J. Lewis-Swan, M. A. Norcia, J. R. K. Cline, J. K. Thompson, and A. M. Rey, Robust Spin Squeezing via Photon-Mediated Interactions on an Optical Clock Transition, Phys. Rev. Lett. **121**, 070403 (2018).

[32] S. L. Zhang and P. van Loock, Local Gaussian operations can enhance continuous-variable entanglement distillation, Phys. Rev. A **84**, 062309 (2011).

[33] C. H. Er, N. N. Chung, and L. Y. Chew, Threshold effect and entanglement enhancement through local squeezing of initial separable states in continuous-variable systems, Phys. Scr. **87**, 025001 (2013).

[34] L. Y. Chew and N. N. Chung, Dynamical relation between quantum squeezing and entanglement in coupled harmonic oscillator system, Symmetry **6**, 295 (2014).

[35] S. K. Joseph, L. Y. Chew, and M. A. Sanjuán, Impact of quantum-classical correspondence on entanglement enhancement by single-mode squeezing, Phys. Lett. A **378**, 2603 (2014).

[36] E. T. S. Ong and L. Y. Chew, The effect of spin squeezing on the entanglement entropy of kicked tops, Entropy **18**, 116 (2016).

[37] M. W. Doherty, F. Dolde, H. Fedder, F. Jelezko, J. Wrachtrup, N. B. Manson, and L. C. L. Hollenberg, Theory of the ground-state spin of the NV^- center in diamond, Phys. Rev. B **85**, 205203 (2012).

[38] R. H. Dicke, Coherence in spontaneous radiation processes, Phys. Rev. **93**, 99 (1954).

[39] D. I. Schuster, A. P. Sears, E. Ginossar, L. DiCarlo, L. Frunzio, J. J. L. Morton, H. Wu, G. A. D. Briggs, B. B. Buckley, D. D. Awschalom, and R. J. Schoelkopf, High-Cooperativity Coupling of Electron-Spin Ensembles to Superconducting Cavities, Phys. Rev. Lett. **105**, 140501 (2010).

[40] Y. Kubo, F. R. Ong, P. Bertet, D. Vion, V. Jacques, D. Zheng, A. Dréau, J.-F. Roch, A. Auffeves, F. Jelezko, J. Wrachtrup, M. F. Barthe, P. Bergonzo, and D. Esteve, Strong Coupling of a Spin Ensemble to a Superconducting Resonator, Phys. Rev. Lett. **105**, 140502 (2010).

[41] M. Tavis and F. W. Cummings, Exact solution for an n-molecule–radiation-field Hamiltonian, Phys. Rev. **170**, 379 (1968).

[42] J. R. Schrieffer and P. A. Wolff, Relation between the Anderson and Kondo Hamiltonians, Phys. Rev. **149**, 491 (1966).

[43] J. M. Luttinger and W. Kohn, Motion of electrons and holes in perturbed periodic fields, Phys. Rev. **97**, 869 (1955).

[44] A. Blais, J. Gambetta, A. Wallraff, D. I. Schuster, S. M. Girvin, M. H. Devoret, and R. J. Schoelkopf, Quantum-information processing with circuit quantum electrodynamics, Phys. Rev. A **75**, 032329 (2007).

[45] S. Bravyi, D. P. DiVincenzo, and D. Loss, Schrieffer-Wolff transformation for quantum many-body systems, Ann. Phys. (NY) **326**, 2793 (2011).

[46] A. Jarmola, V. M. Acosta, K. Jensen, S. Chemerisov, and D. Budker, Temperature- and Magnetic-Field-Dependent Longitudinal Spin Relaxation in Nitrogen-Vacancy Ensembles in Diamond, Phys. Rev. Lett. **108**, 197601 (2012).

[47] R. Hanson, V. V. Dobrovitski, A. E. Feiguin, O. Gywat, and D. D. Awschalom, Coherent dynamics of a single spin interacting with an adjustable spin bath, Science **320**, 352 (2008).

[48] L. Childress, M. V. Gurudev Dutt, J. M. Taylor, A. S. Zibrov, F. Jelezko, J. Wrachtrup, P. R. Hemmer, and M. D. Lukin, Coherent dynamics of coupled electron and nuclear spin qubits in diamond, Science **314**, 281 (2006).

[49] G. de Lange, Z. H. Wang, D. Ristè, V. V. Dobrovitski, and R. Hanson, Universal dynamical decoupling of a single solid-state spin from a spin bath, Science **330**, 60 (2010).

[50] C. A. Ryan, J. S. Hodges, and D. G. Cory, Robust Decoupling Techniques to Extend Quantum Coherence in Diamond, Phys. Rev. Lett. **105**, 200402 (2010).

[51] B. Naydenov, F. Dolde, L. T. Hall, C. Shin, H. Fedder, L. C. L. Hollenberg, F. Jelezko, and J. Wrachtrup, Dynamical decoupling of a single-electron spin at room temperature, Phys. Rev. B **83**, 081201(R) (2011).

[52] E. Bauch, C. A. Hart, J. M. Schloss, M. J. Turner, J. F. Barry, P. Kehayias, S. Singh, and R. L. Walsworth, Ultralong Dephasing Times in Solid-State Spin Ensembles via Quantum Control, Phys. Rev. X **8**, 031025 (2018).

[53] B.-B. Wei, C. Burk, J. Wrachtrup, and R.-B. Liu, Magnetic ordering of nitrogen-vacancy centers in diamond via resonator-mediated coupling, EPJ Quantum Technol. **2**, 18 (2015).

[54] A. B. Hutchinson, P. A. Truitt, K. C. Schwab, L. Sekaric, J. M. Parpia, H. G. Craighead, and J. E. Butler, Dissipation in nanocrystalline-diamond nanomechanical resonators, Appl. Phys. Lett. **84**, 972 (2004).

[55] M. K. Zalalutdinov, M. P. Ray, D. M. Photiadis, J. T. Robinson, J. W. Baldwin, J. E. Butler, T. I. Feygelson, B. B. Pate, and B. H. Houston, Ultrathin single crystal diamond nanomechanical dome resonators, Nano Lett. **11**, 4304 (2011).

[56] P. Ovartchaiyapong, L. M. A. Pascal, B. A. Myers, P. Lauria, and A. C. Bleszynski Jayich, High quality factor single-crystal diamond mechanical resonators, Appl. Phys. Lett. **101**, 163505 (2012).

[57] Y. Tao, J. M. Boss, B. A. Moores, and C. L. Degen, Single-crystal diamond nanomechanical resonators with quality factors exceeding one million, Nat. Commun. **5**, 3638 (2014).

[58] G. Vidal and R. F. Werner, Computable measure of entanglement, Phys. Rev. A **65**, 032314 (2002).

[59] M. B. Plenio, Logarithmic Negativity: A Full Entanglement Monotone that is not Convex, Phys. Rev. Lett. **95**, 090503 (2005).

[60] K. Audenaert, M. B. Plenio, and J. Eisert, Entanglement Cost under Positive-Partial-Transpose-Preserving Operations, Phys. Rev. Lett. **90**, 027901 (2003).

[61] T. Holstein and H. Primakoff, Field dependence of the intrinsic domain magnetization of a ferromagnet, Phys. Rev. **58**, 1098 (1940).

[62] S. M. Barnett and P. M. Radmore, *Methods in Theoretical Quantum Optics* (Clarendon, Oxford, 1997), Chap. 4, p. 106.

[63] C. W. Gardiner and P. Zoller, *Quantum Noise* (Springer, Berlin, 1999).

[64] L.-M. Duan, G. Giedke, J. I. Cirac, and P. Zoller, Inseparability Criterion for Continuous Variable Systems, Phys. Rev. Lett. **84**, 2722 (2000).

[65] R. Simon, Peres-Horodecki Separability Criterion for Continuous Variable Systems, Phys. Rev. Lett. **84**, 2726 (2000).

[66] J. N. Bandyopadhyay and A. Lakshminarayan, Testing Statistical Bounds on Entanglement Using Quantum Chaos, Phys. Rev. Lett. **89**, 060402 (2002).

[67] D. J. Christle, P. V. Klimov, C. F. de las Casas, K. Szász, V. Ivády, V. Jokubavicius, J. Ul Hassan, M. Syväjärvi, W. F. Koehl, T. Ohshima, N. T. Son, E. Janzén, A. Gali, and D. D. Awschalom, Isolated Spin Qubits in SiC with a High-Fidelity Infrared Spin-to-Photon Interface, Phys. Rev. X **7**, 021046 (2017).

[68] G. E. Uhlenbeck and L. S. Ornstein, On the theory of the Brownian motion, Phys. Rev. **36**, 823 (1930).

[69] P. W. Anderson and P. R. Weiss, Exchange narrowing in paramagnetic resonance, Rev. Mod. Phys. **25**, 269 (1953).

[70] J. R. Klauder and P. W. Anderson, Spectral diffusion decay in spin resonance experiments, Phys. Rev. **125**, 912 (1962).